AGU ADVANCING EARTH AND SPACE SCIENCES

JAMES | Journal of Advances in Modeling Earth Systems®

RESEARCH ARTICLE
10.1029/2024MS004441

Modeling Thermal and Biogeochemical Dynamics in Two Ponds Within Alaska's Yukon–Kuskokwim Delta: Impacts of Climatic Variability on Greenhouse Gas Fluxes

A. L. Mullen[1], E. E. Jafarov[1], J. K. Y. Hung[1], K. Gurbanov[1], V. Stepanenko[2,3], B. M. Rogers[1], J. D. Watts[1], S. M. Natali[1], and B. A. Poulin[4]

[1]Woodwell Climate Research Center, Falmouth, MA, USA, [2]Lomonosov State University, Moscow, Russia, [3]Moscow Center of Fundamental and Applied Mathematics, Moscow, Russia, [4]Department of Environmental Toxicology, University of California Davis, Davis, CA, USA

Key Points:

- LAKE model simulations indicate that snow cover, ice duration, and water temperatures play an important role in greenhouse gas dynamics
- Removal of snow cover slightly increased water body CH_4 and CO_2 fluxes
- A 2.7 C increase in air temperature led to a 5% increase water body CH_4 emissions and 12% increase in water body CO_2 emissions

Supporting Information:

Supporting Information may be found in the online version of this article.

Correspondence to:

E. E. Jafarov,
ejafarov@woodwellclimate.org

Citation:

Mullen, A. L., Jafarov, E. E., Hung, J. K. Y., Gurbanov, K., Stepanenko, V., Rogers, B. M., et al. (2025). Modeling thermal and biogeochemical dynamics in two ponds within Alaska's Yukon–Kuskokwim Delta: Impacts of climatic variability on greenhouse gas fluxes. *Journal of Advances in Modeling Earth Systems*, *17*, e2024MS004441. https://doi.org/10.1029/2024MS004441

Received 1 JUN 2024
Accepted 8 APR 2025

Author Contributions:

Conceptualization: E. E. Jafarov
Data curation: A. L. Mullen, E. E. Jafarov, J. K. Y. Hung, K. Gurbanov
Formal analysis: A. L. Mullen, E. E. Jafarov
Funding acquisition: E. E. Jafarov, V. Stepanenko, B. M. Rogers, J. D. Watts, S. M. Natali, B. A. Poulin
Investigation: A. L. Mullen, E. E. Jafarov, J. K. Y. Hung, K. Gurbanov, V. Stepanenko

Abstract Fluxes of carbon dioxide (CO_2) and methane (CH_4) from open water bodies are critical components of carbon-climate feedbacks in high latitudes. Processes governing the spatial and temporal variability of these aquatic greenhouse gas (GHG) fluxes are still highly uncertain due to limited observational data sets and lack of modeling studies incorporating comprehensive thermal and biochemical processes. This research investigates how slight variations in climate propagate through the biogeochemical cycles of ponds and resulting impacts on GHG emissions. We examine the thermal and biogeochemical dynamics of two ponds in the Yukon–Kuskokwim Delta, Alaska, under varying climatic conditions to study the impacts on CO_2, CH_4, and oxygen (O_2) concentrations and fluxes. We performed multiple numerical experiments, using the LAKE process-based model and field measurements, to analyze how these ponds respond to variations in air temperature, shortwave radiation, and snow cover. Our study demonstrates that ice cover duration and water temperature are primary climatic drivers of GHG fluxes. Climate experiments led to reductions in ice cover duration and increased water temperatures, which subsequently enhanced CH_4 and CO_2 gas emissions from two study ponds. On average, cumulative CH_4 and CO_2 emissions were 5% and 10% higher, respectively, under increases in air temperature and shortwave radiation. Additionally, we uncovered a need to incorporate groundwater influxes of dissolved gases and nutrients in order to fully represent processes governing aquatic biochemical activity. Our work highlights the importance of understanding local-scale processes in predicting future Arctic contributions to GHG emissions.

Plain Language Summary Quantifying the release of carbon dioxide (CO_2) and methane (CH_4) from Arctic lakes is one of the major uncertainties in the carbon budget of the Arctic. However, it is challenging to quantify due to the limited data and lack of models that include detailed thermal and biochemical processes. We explored how climatic variables impact the way ponds produce and emit greenhouse gases (GHGs). We studied two ponds in Alaska's Yukon-Kuskokwim Delta using field data and a computer model to understand how changes in air temperature, sunlight, and snow cover influence CO_2, CH_4, and oxygen levels. We found that the duration of ice cover and water temperature are key climate factors influencing gas emissions. Warmer temperatures and increased sunlight reduce ice cover and heat up the water, resulting in higher emissions of CH_4 and CO_2 from the ponds. Under warmer conditions, cumulative emissions of methane and carbon dioxide increased by 5% and 10%, respectively, compared to baseline conditions. Future models need to include groundwater influxes of dissolved gases and nutrients for a complete understanding of these complex biochemical processes. Our study emphasizes the need to understand local processes to better predict the Arctic's future contribution to global GHG emissions.

1. Introduction

Ponds and lakes (i.e., water bodies) in the Arctic and sub-Arctic account for nearly two-thirds of all natural methane (CH_4) sources in the region and are highly sensitive to changes in climate (Wik et al., 2016). The emission of CH_4 from Arctic water bodies ranges from 3 to 18 Tg CH_4 per year, with the broader region contributing 25 to 240 Tg of carbon dioxide (CO_2) annually (Matthews et al., 2020; Ramage et al., 2024). Northern high latitudes are warming at a rapid rate compared with other regions (Ballinger et al., 2024; Constable et al., 2022), with Arctic air temperatures anticipated to increase by 3.3–10°C above the 1985–2014 mean by the end of the century (AMAP, 2021). These changes in climate will increase water temperatures and reduce ice cover

Methodology: A. L. Mullen, E. E. Jafarov, J. K. Y. Hung, K. Gurbanov, V. Stepanenko, B. M. Rogers
Project administration: E. E. Jafarov, B. A. Poulin
Resources: E. E. Jafarov
Software: A. L. Mullen, E. E. Jafarov, K. Gurbanov, V. Stepanenko, B. M. Rogers
Supervision: E. E. Jafarov
Validation: A. L. Mullen, E. E. Jafarov, K. Gurbanov, V. Stepanenko, B. M. Rogers
Visualization: A. L. Mullen, E. E. Jafarov
Writing – original draft: A. L. Mullen, E. E. Jafarov
Writing – review & editing: A. L. Mullen, E. E. Jafarov, J. K. Y. Hung, K. Gurbanov, V. Stepanenko, B. M. Rogers, J. D. Watts, S. M. Natali, B. A. Poulin

durations, enhancing microbial activity and production of CH_4 in the water column and bottom sediments (Wik et al., 2016). Increases in terrestrial primary productivity (Elmendorf et al., 2012; Pouliot et al., 2009) and encroachment of emergent vegetation into ponds as they dry (Finger Higgens et al., 2019) are also anticipated to enhance the production and evasion of CH_4 from water bodies (Rehder et al., 2023). Permafrost thaw and talik development (unfrozen ground that remains year-round), are accelerated after high latitude disturbance events (i.e., wildfire) (Abbott et al., 2016; Jafarov et al., 2013), delivering carbon into water bodies and increasing microbial respiration (Prėskienis et al., 2024). Enhanced interactions between surface water and groundwater will also amplify greenhouse gas (GHG) emissions from open water bodies (Abnizova et al., 2012; Arp et al., 2011; Jeffries et al., 1999; Jorgenson & Shur, 2007; M. T. Jorgenson et al., 2006; Prėskienis et al., 2024; Rouse et al., 1997; Rowland et al., 2011; Wik et al., 2016). Small water bodies (<0.1 km^2) are particularly potent CH_4 emitters across the Arctic and sub-Arctic, comprising ∼12% of water body area and ∼30% of total open water methane emissions (Kyzivat & Smith, 2023). In tundra delta environments such as the Yukon-Kuskokwim Delta (YKD), the contributions of small water bodies are potentially greater, comprising ∼46% of open water area and ∼52% of open water CH_4 emissions (Ludwig et al., 2023). Small water bodies are also important contributors to CO_2 fluxes in high latitude tundra environments. Studies from the Lena River Delta found that small water bodies produce over 70% of CO_2 outflux (Abnizova et al., 2012), and significantly reduce the CO_2 sink of the overall landscape (Beckebanze et al., 2022). However, wildfire reduction of carbon stocks can reduce CO_2 inputs in waterbodies and have mixed results for CH_4, driven by the surrounding land cover (Zolkos et al., 2022).

Increases in GHG emissions from high-latitude water bodies could contribute to a significant amplification in warming. Previous studies have estimated Arctic water body contributions to GHG budgets at various spatial scales through statistical upscaling (Saunois et al., 2020) and process modeling (Johnson et al., 2022; Tan & Zhuang, 2015a; Zhuang et al., 2023). However, the processes driving the spatial and temporal variability are still poorly constrained. Therefore, improving understanding of the processes that regulate CH_4 production and emissions at a local scale is critical. Process-based models provide insights into the spatiotemporal variability of GHG fluxes that is currently poorly constrained by field measurements that are often collected at discrete points in time and often restricted to the warm season. Some year round observations of water body CO_2 and CH_4 fluxes exist, but comprehensive measurement is hindered by uncertainties in capturing the significant fluxes that can be released during ice breakup (Jammet et al., 2017; Prėskienis et al., 2021). As a result, many statistical GHG flux upscaling studies only provide single snapshots in time (Ludwig et al., 2023; Rosentreter et al., 2021; Stackpoole et al., 2017). Model simulations of GHG fluxes are needed to fill observational gaps and provide time-integrated estimates of cumulative emissions.

One-dimensional coupled thermal-biogeochemical models are critically useful for predicting GHG emissions from ponds because they strike a balance between comprehensive process representation and computational efficiency that allows for both representativeness at the site-level and upscaling to broader areas (Grant et al., 2021). Various one-dimensional models have been used to represent the thermal and biological processes of high-latitude water bodies. The Arctic Lake Biochemistry Model (Tan et al., 2015, 2017) has been used to assess the impacts of warming air temperature on global and high-latitude CH_4 emissions (Guo et al., 2020; Zhuang et al., 2023). Rehder et al. (2023) developed the Methane Emissions from Ponds (MeEP) model to quantify changes in polygonal tundra pond methane production and emissions pathways with warming climate and increasing terrestrial input of labile organic carbon. The LAKE model (Stepanenko et al., 2016, 2020), has been tested across different climate conditions in projects like the Lake Model Intercomparison Project (LakeMIP; Stepanenko et al., 2014), and validated against observations in high-latitude lakes (Clark et al., 2022) and reservoirs (Lomov et al., 2023).

Despite these advancements in lake modeling, gaps remain in the understanding of the impact of drivers such as water temperatures, ice thickness, and snow depth on GHG emissions from Arctic lakes (Clark et al., 2022; Jeffries & Morris, 2006; Rantanen et al., 2022). Additionally, very few studies assess the thermal and biogeochemical dynamics of small ponds for both ice-on and ice-free seasons. This study addresses these gaps by focusing on the interactions between thermal and biogeochemical processes under different climatic conditions. The primary goal of this study is to advance our understanding of how different climatic drivers influence GHG (CO_2 and CH_4) and oxygen (O_2) dynamics in Arctic pond ecosystems. The study is driven by the hypothesis that variations in climate, such as increases in air temperature or changes in snow and ice cover, can significantly alter the thermal regime of pond waters and, thus, the associated GHG dynamics. We utilize meteorological and biogeochemical data collected at two ponds in the Yukon-Kuskokwim Delta, Alaska, to conduct numerical

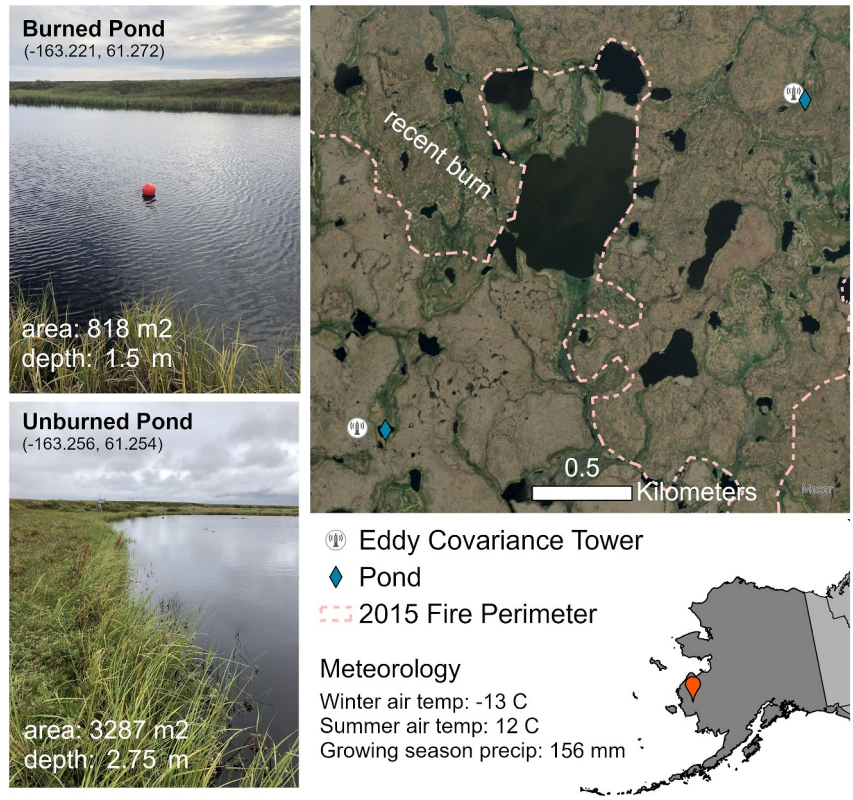

Figure 1. Photos and locations of the two studied ponds in the Yukon–Kuskokwim Delta, Alaska. One pond is located within the perimeter of a 2015 wildfire (Burned Pond) and the other pond is located in unburned tundra (Unburned Pond).

simulations to study climate impacts on water thermal and biogeochemical conditions. We use LAKE, a one-dimensional physics-based numerical model that integrates both thermodynamic and biogeochemical processes, to assess the sensitivity of lake water temperature, ice thickness, and snow depth to climatic variations in the Arctic. In addition, we show the contribution of different production mechanisms to the cumulative emission of GHGs in two ponds.

2. Materials and Methods

2.1. Study Site

The Yukon-Kuskokwim Delta (YKD) of southwestern Alaska is underlain by discontinuous permafrost and characterized by sedge, moss, and low-shrub peat plateaus interspersed with small lakes, ponds, streams, bogs, and fens (Figure 1). The 2015 fire season in Alaska was the second largest on record with 21,000 km^2 burned, of which roughly 542 km^2 occurred within the YKD (Moubarak et al., 2023). Research has been conducted within 10 km of these lakes since 2015 investigating permafrost thaw and wildfire effects on carbon cycling, vegetation, and aquatic ecosystems (Baillargeon et al., 2022; Dabrowski et al., 2020; Frost et al., 2020; Ludwig et al., 2022, 2023, 2024; Michaelides et al., 2019; Moubarak et al., 2023; Mullen et al., 2023; Sae-Lim et al., 2019; Zolkos et al., 2022). Mean growing season (June, July, August) air temperature in 2022 was 12.3°C, while mean cold season air temperature (December, January, February) was −12.6°C. Growing season precipitation in 2022 totaled 156 mm. Maximum summer thaw depths in 2022 reached 75 cm in unburned tundra and 91 cm in burned tundra.

2.2. Data Collection

As part of the ongoing research in the watershed, two eddy covariance (EC) towers measuring high frequency CO_2 and CH_4 fluxes and meteorological variables were established in July 2019 and September 2019 on unburned and burned tundra, respectively. Data collected from the EC towers for model input included half-hourly

meteorological variables, including air temperature, air pressure, relative humidity, longwave radiation, shortwave radiation, precipitation rate, wind speed, and wind direction. Detailed information on EC tower instrumentation and data processing can be found in Ludwig et al. (2024).

Within the tower footprints, two ponds (unburned: −163.256°E, 61.254°N; and burned: −163.221°E, 61.272°N) were selected as part of this study: the unburned pond has a surface area of 3,287 m^2, with a depth of 2.75 m, while the burned pond covers an area of 818 m^2 with a depth of 1.5 m (Figure 1). Each pond was instrumented during the 2022 growing season (late June to mid-August) with a dual range eosGP gas probe (Eosense Inc., Dartmouth, Nova Scotia, Canada) connected to a CR1000X data logger (Campbell Scientific Inc., Logan, Utah, USA) measuring continuous half-hourly CO_2 concentrations and water temperature. The eosGP sensors were calibrated for a 0 to 20,000 ppm range (±3.5% accuracy) prior to deployment, and deployed at about 1 m below the pond surface and connected to a surface buoy anchored to the pond bottom to prevent movement within the pond.

Surface water samples were collected weekly during the 2022 growing season (late June to early September) from identical shoreline locations at each of the unburned and burned ponds and analyzed for biogeochemical variables. At each sampling time point, in situ water temperature (°C), pH, electrical conductivity (μS cm^{-1}), and dissolved O_2 (mg L^{-1}) were measured using a Professional-Plus water quality sonde that was calibrated daily (Yellow Springs Instruments, Yellow Spring, Ohio, USA). Dissolved gases (CO_2 and CH_4) were collected using the headspace equilibration method (Hesslein et al., 1991), where 30 mL of water and 30 mL of atmospheric air were shaken for 1 min within a sealed polypropylene syringe before injection into a pre-evacuated 12 mL Exetainer vial sealed with a butyl septum. Dissolved gas samples were analyzed within four weeks of collection by gas chromatography equipped with a flame ionization detector (GC-2014, Shimadzu Scientific Instruments, Kyoto, Japan) at the Woodwell Climate Research Center Environmental Chemistry Laboratory. Additionally, dissolved organic carbon (DOC) and total dissolved nitrogen (TDN) were analyzed for. Methods for surface water filtration and laboratory analysis followed Zolkos et al. (2022).

2.3. Data Processing

EC tower meteorological variables were aggregated daily and gap-filled to drive the LAKE model (Figure 2). Between July and September 2022, there was no missing meteorological data at the burned tower, whereas 29% of days in the same period had at least one meteorological variable missing at the unburned tower. Data gaps in one tower's data were filled using bias-corrected data from the other tower (Figure S1 in Supporting Information S1). Bias corrections were determined based on linear regressions between burned and unburned tower data for the respective variables. This method resulted in only 9 days of missing data, which were filled using linear interpolation between the nearest 2 days of available data. As no snow depth information was collected at either pond, snow-water equivalent (SWE) accumulation rates were derived from the McGrath automated snow telemetry (SNOTEL) monitoring site (−155.37°W, 62.57°N; 850 km from field area). The SNOTEL SWE depths were adjusted with a simple multiplier (0.5) to align the data with expected snow depths over each pond based on in situ snow depth measurements (i.e., snow depth probing) from 3 years of wintertime site visits. To quantify uncertainty in snowfall driving data, the modeled snow appearance and disappearance dates were validated using remotely sensed snow cover fraction from the Visible Infrared Imaging Radiometer Suite (VIIRS) Level 3 daily cloud gap-filled 375 m snow cover product (VNP10A1F; Riggs et al., 2015). This product quantifies the fractional surface area of each pixel that is snow-covered (0%–100%; see Text S4 and Figure S2 in Supporting Information S1 for more detail).

2.4. Model Description and Setup

Over the last 20 years, the LAKE model has been developed to predict carbon cycling and GHG emissions in global water bodies using meteorological measurements (Lomov et al., 2023; Stepanenko & Lykossov, 2005; Stepanenko et al., 2016). The LAKE model is an extended one-dimensional model that simulates thermodynamic, hydrodynamic, and biogeochemical processes in water basins and sediments. Despite the one-dimensional nature of the model, it takes into account the lake/pond morphometry and water thermal and biogeochemical conditions accordingly. It considers factors like heat transfer, radiation penetration, ice, snow, and sediment dynamics. The model also accounts for ice evolution in frozen lake waters and soils. Equations in the model are formulated for averaged quantities across the water body's horizontal section, explicitly considering momentum, heat, and gas exchange. It addresses turbulence, pressure gradients, heat and liquid water transport in ice and snow, water phase

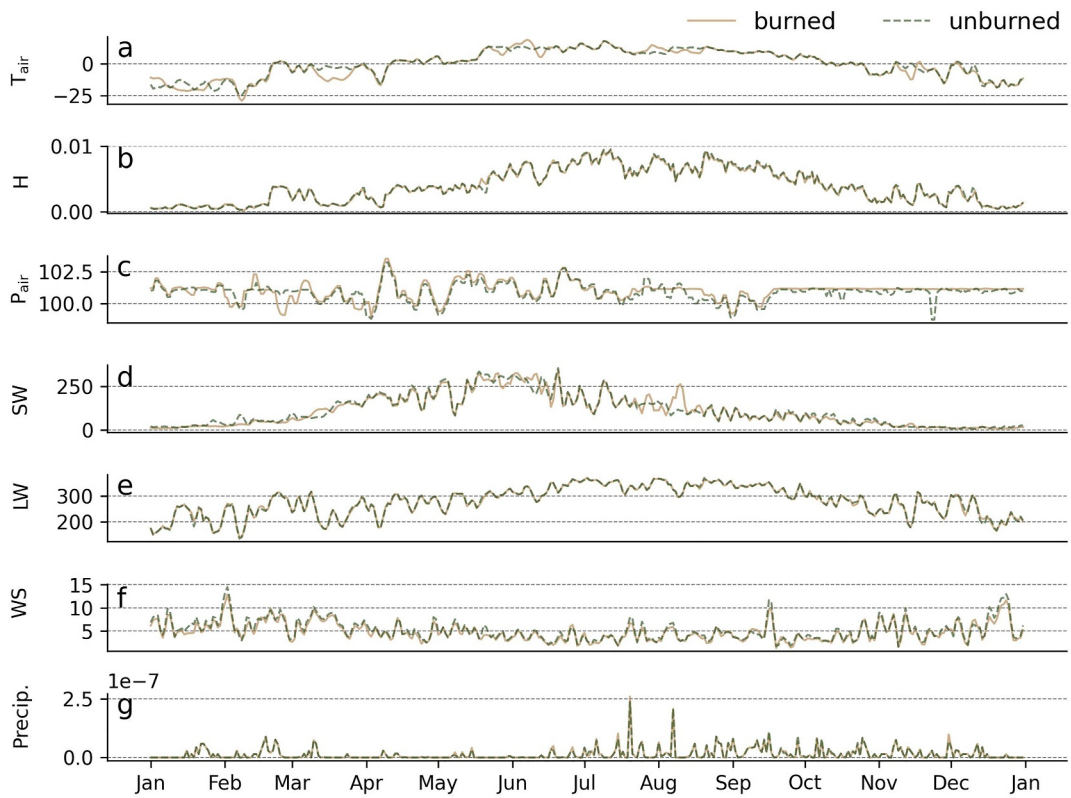

Figure 2. Daily meteorological data from 2022 used in simulations for burned and unburned ponds in the Yukon–Kuskokwim Delta. Air temperature (T_{air}; C) (a), humidity (H; kg kg^{-1}) (b), atmospheric pressure (P_{air}; kPa) (c), shortwave radiation (SW; W m^{-2}) (d), longwave radiation (LW; W m^{-2}) (e), wind speed (WS; m s^{-1}) (f), and precipitation (Precip; m s^{-1}) (g).

changes in sediments, and the vertical diffusion and ebullition of dissolved gases (CH_4, CO_2, and O_2). The model has been tested across different climate conditions in projects like the Lake Model Intercomparison Project (LakeMIP; Stepanenko et al., 2014). More recently, the model was validated on three lakes in North Slope, Alaska (Clark et al., 2022).

The LAKE model (v3.0) was run at a one-day timestep. The water column was broken into 40 vertical layers, ice and soil were broken into 10 vertical layers respectively, and the soil is divided horizontally with five soil columns. In the absence of soil core data, soil was inferred to have a silt loam texture based on soil maps from Jorgenson et al. (2008) and the U.S. Department of Agriculture STATSGO2 product (USDA, 2017). Water-atmosphere heat flux parameterization used the formulation from FLake (Mironov, 2008; Mironov et al., 2009), and the turbulent mixing used the K-epsilon parameterization. Mass flux (convection) was represented using the Siebesma et al. (2007) parameterization. The extinction coefficient of water was set to 0.5 based on observations from similar high-latitude water bodies (Seekell et al., 2015). Inflows of water, chemical, and particulate constituents were not accounted for in the model configurations. The ponds have no aboveground tributary streams, but groundwater flows could still influence pond processes.

We spun up the LAKE model until we reached steady yearly fluxes and concentrations of heat and gases in the water and soil. The data for spin-up was generated by repeating the daily time series from 2022 for each pond over 40 years, based on the in situ data availability. To reduce the compute time, we smoothed spin-up data using a Savitzky-Golay filter over a 25-day moving window. This prolonged spin-up duration was essential for achieving stable contemporary model runs. Given that 2022 air temperatures were only slightly colder than the 1991–2022 average for the growing season (~0.2°C) and cold season (~1°C) (NOAA, 2022), the limited temporal extent of the spin-up data could have led to slightly colder deep (>1 m) soil layers that contribute minimally to biogeochemical processes in the model experiments.

Table 1
Values and Ranges of Six Parameters Used in Parameter Sensitivity Analysis and Climate Experiments

	Burned		Unburned		
Parameter	Value	Range tested	Value	Range tested	Sources
V_{max} (mol m^{-3} s^{-1})	1.15E–07	1.0E–10, 8.0E–5	1.15E–07	1.0E–10, 8.0E–5	Lidstrom and Somers (1984), Liikanen et al. (2002)
$K_{hs,CH4}$ (mol m^{-3})	3.75E–02	1.0E–4, 5.0E–1	3.75E–02	1.0E–4, 5.0E–1	Lidstrom and Somers (1984), Liikanen et al. (2002)
$K_{hs,O2}$ (mol m^{-3})	2.10E–02	5.0E–7, 5.0E–1	2.10E–02	5.0E–7, 5.0E–1	Lidstrom and Somers (1984), Watson et al. (1997)
R_0 (mol m^{-3} s^{-1})	8.50E–08	5.0E–11, 9.0E–6	4.30E–08	5.0E–11, 9.0E–6	Stepanenko et al. (2016)
$k_{c,0}$ (m s^{-1})	5.68E–07	5.0E–9, 5.0E–5	3.44E–07	1.0E–8, 5.0E–4	Walker and Snodgrass (1986)
$\mu_{\beta,0}$ (mol m^{-2} s^{-1})	1.70E–06	5.0E–7, 6.0E–5	6.50E–06	5.0E–7, 6.0E–4	Walker and Snodgrass (1986)

Note. V_{max}(mol m^{-3} s^{-1}): Maximal methane aerobic oxidation rate, $K_{hs,CH4}$ (mol m^{-3}): half-saturation constant for CH_4, $K_{hs,O2}$ (mol m^{-3}): half-saturation constant for O_2, R_0 (mol m^{-3} s^{-1}): constant controlling the magnitude of methane production in sediments, $k_{c,0}$ (m s^{-1}): the mass transfer coefficient, $\mu_{\beta,0}$ (mol m^{-2} s^{-1}): coefficient proportional to organics oxidation potential rate in sediments.

2.5. Model Parameter Calibration

To tune the model to match measured CH_4, CO_2, and O_2 concentrations, we ran sensitivity analyses on six parameters, as documented in Table 1. The model was run repeatedly while varying the calibration parameters, and the parameter set producing the best match with observations was identified for each pond. The calibration parameters were chosen based on their impact on CH_4 production, oxidation, and transport, and CO_2 production and transport (Stepanenko et al., 2016) (see Supporting Information S1). R_0 is the CH_4 base production rate with respect to methanogenesis in sediments, reflecting the quantity and quality of new organic material prone to anaerobic decomposition (Equation S1 in Supporting Information S1). The V_{max}, $K_{hs,O2}$ and $K_{hs,CH4}$ are reaction potential and two half-saturation constants controlling aerobic CH_4 oxidation in the water column (Equations S2 and S3 in Supporting Information S1). In LAKE, aerobic CH_4 oxidation also occurs in the top ∼1 cm of soil (Equation S4 in Supporting Information S1). Parameters governing CH_4 oxidation in the soil were not calibrated, following (Stepanenko et al., 2016). The last two parameters are constants that impact the sedimentary oxygen demand function, diffusion, and biochemical consumption (Equations S5–S7 in Supporting Information S1). $\mu_{\beta,0}$ is a multiplier in the potential rate of microbial decomposition in aerobic sediments, and $k_{c,0}$ is constant reference diffusivity for CO_2 transfer between sediments and water, respectively (Walker & Snodgrass, 1986). Further information on the multiprocessing technique and equations associated with the tuned parameters is provided in Texts S1 and S2 in Supporting Information S1.

Each sensitivity analysis run was initialized with temperature and biogeochemical profiles from the 40-year spinup run for each pond. We used a random logarithmic-uniform distribution method to sample parameters within the given ranges shown in Table 1. To provide time for the model to re-equilibrate with the new parameter sets, we ran the model for 18 months. Comparisons to observations used model outputs from the final year of each sensitivity run. After each parameter sensitivity run, we updated the ranges to allow a better match with observational data. Final parameters were selected based on values that produced the highest R^2 and lowest mean absolute error (MAE) between modeled and observed water temperatures and concentrations of CH_4, CO_2, and O_2.

2.6. Primary Production

Primary production has the potential to influence gas concentrations and fluxes in the two ponds. Although the study ponds did not have significant vascular aquatic vegetation, which has been shown to facilitate GHG ebullition (Knoblauch et al., 2015), phytoplankton species likely conduct photosynthesis at a non-negligible rate (Maeda et al., 2019). We use trophic state index (TSI) as an indicator of primary productivity in the comparison of model data to observations. We calculate modeled TSI using chlorophyll-a following (Carlson, 1977) (Equation S8 in Supporting Information S1). Since we did not have direct observations of photosynthesis or chlorophyll-a content, we calculated the observed TSI using TDN measurements following (Kratzer & Brezonik, 1981) (Equation S9 in Supporting Information S1). While this comparison is indirect, nitrogen has been shown to be a good indicator of trophic state and phytoplankton content (Aizaki et al., 1981; Hu et al., 2021; Jensen et al., 2019).

2.7. Setup for Model Sensitivity to Meteorological Inputs

After biogeochemical parameters were calibrated to match observations at each pond, three experiments were carried out to explore model sensitivity to varying meteorological inputs.

2.7.1. Snowfall Removal

For the no-snow (NS) experiment, all snowfall was removed, and rain remained unaltered to explore the insulating effect of snow on water and sediment temperatures and the resulting biogeochemistry. The role of snow and ice in influencing lake water and biogeochemistry is critical in sub-Arctic environments characterized by discontinuous and sporadic permafrost. In many cases, lakes with depths up to 2 m are expected to refreeze entirely to the bottom during winter, as observed in regions such as the North Slope (e.g., Arp et al., 2012; Arp et al., 2018). However, the inability of shallow lakes to refreeze completely has profound implications for permafrost stability. Without a fully frozen lake bottom, heat transfer from unfrozen water to underlying sediments persists throughout the winter, driving the expansion of thaw bulbs beneath the lake. This process accelerates permafrost degradation, particularly in regions where hydrological connectivity further enhances heat and nutrient transport. Continuous wintertime thawing beneath these lakes could lead to widespread permafrost destabilization, with cascading impacts on carbon cycling, as thawing sediments release stored organic matter into the aquatic system (Walter Anthony et al., 2018).

2.7.2. Shortwave Radiation

For the shortwave radiation (SW20) experiment, downward shortwave radiation was increased by 20%, which increased average yearly solar radiation by ∼20 W m^{-2}. Shortwave radiation varies considerably with latitude in the Arctic and sub-Arctic (Hatzianastassiou et al., 2005), and maximum yearly average incoming shortwave radiation is ∼20 W m^{-2} greater than that of the study area for the latitudes spanning Alaska (Dissing & Wendler, 1998). Thus, the SW20 experiment is intended to address the spatial variability of shortwave radiation across high-latitude regions. Shortwave radiation impacts biogeochemical cycles by altering thermal regimes, primary productivity, and photodegradation of organic matter. Shortwave radiation provides a significant source of heat for sediments that can be linked to the intensity of CH_4 emissions (Liu & Zhuang, 2023; Wik et al., 2016). Increased shortwave radiation can have varying impacts on the balance of CO_2 consumption through photosynthesis (Megard et al., 1984) and CO_2 production through microbial and photochemical pathways (Jansen et al., 2019; Koehler et al., 2014).

2.7.3. Air Temperature

For the air temperature (TA1) experiment, air temperature was increased by 1%, which corresponded to the overall increase in mean annual air temperature by ∼2.7°C, slightly higher than used by Clark et al. (2022). It is well known that rising mean annual air temperatures in the Arctic are profoundly altering lake systems, impacting both their physical state and biogeochemistry. While this 2.7°C air temperature increase is lower than the minimum anticipated 3.3°C increase by 2100 under Shared Socioeconomic Pathway 1–2.6 (AMAP, 2021), it illustrates the widespread effects of small perturbations in this dominant climate variable. Higher air temperatures result in warmer waters that promote the release of CH_4 and CO_2 from lake sediments, as microbial decomposition of organic matter accelerates (Walter Anthony et al., 2018). In the small and shallow lake this response of temperature warming to the entire water column is immediate. Higher water temperatures increase permafrost thaw around lake margins, delivering organic matter and nutrients into the lakes, which can alter nutrient cycling and enhance GHG emissions (Eugster et al., 2022; Prėskienis et al., 2024). The cumulative effects of warming thus position Arctic lakes as critical nodes in the global carbon cycle, amplifying feedback loops that further accelerate climate change.

3. Results

3.1. Modeled and Observed Data Comparison

3.1.1. Water Temperature and Snow Cover

Figures 3a and 3b show the results of the modeled water temperature compared with observations at the two ponds at a 1 m depth. In general, the modeled temperatures were in agreement with the observed temperatures. The MAE

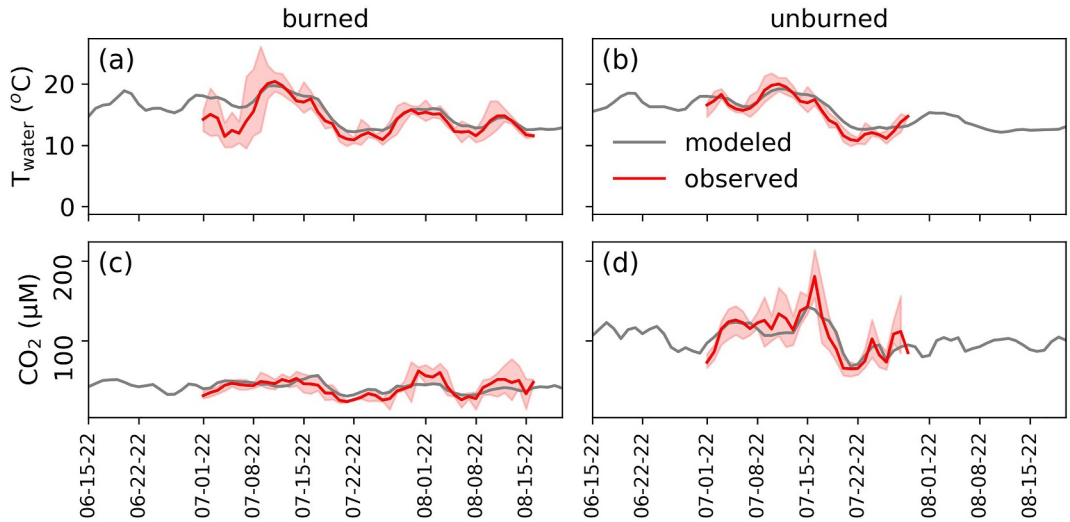

Figure 3. Comparison of modeled (gray) and observed (red) water temperatures at the burned (a) and unburned (b) ponds at a 1 m depth. Comparison of modeled (gray) and observed (red) water CO_2 concentrations at the burned (c) and unburned (d) ponds at a 1 m depth. The solid red line is the daily mean of 30-min water temperature and CO_2 measurements, calculated for direct comparison with model outputs at a daily timestep. The light red shading indicates the variability at the 95% confidence interval of the water temperatures and CO_2 concentrations measured throughout each day.

was 1.1°C and 1.2°C for the unburned and burned ponds, respectively. The coefficients of determination (R^2) between modeled and observed water temperatures were 0.82 and 0.52 for the unburned and burned ponds, respectively.

Compared with remotely sensed snow cover fraction from VIIRS, modeled snow appearance aligned within 9 days and snow disappearance aligned within 4 days. Figure S2 in Supporting Information S1 shows the time series of VIIRS snow cover fraction used to determine the alignment.

3.1.2. CO_2, O_2, and CH_4 Concentrations

The R_0 parameter, which controls the magnitude of CH_4 production in sediments, had the greatest effect on CH_4 concentrations and was the focus of model tuning to match observed CH_4 concentrations. The top-performing sensitivity analysis runs used R_0 values of 0.085 and 0.043 μmol m^{-3} s^{-1} for the burned and unburned ponds, respectively. The maximum rate of oxidation (V_{max}) also affected CH_4 concentrations and needed to be quite low (0.115 μmol m^{-3} s^{-1}) for both ponds to match the observed CH_4 concentrations. Given the low CH_4 oxidation potential calibrated through V_{max}, adjustments of the Michaelis-Menten half-saturation concentrations $K_{hs,O2}$ and $K_{hs,CH4}$ did not noticeably improve the agreement between modeled and measured CH_4 concentrations. We elected to use the values for these parameters from Lidstrom and Somers (1984), Liikanen et al. (2002), and Lofton et al. (2014). Similarly, the reference diffusivity for CO_2 transfer between sediments and water ($k_{c,0}$) was calibrated but had a minimal effect on the CO_2 concentrations. The $\mu_{\beta,0}$ parameter, which controls sediment aerobic oxidation rates, had the greatest effect on CO_2 concentrations and emphasis was placed on tuning this parameter to match observed CO_2 concentrations. Top performing sensitivity analysis runs used $\mu_{\beta,0}$ values of 1.7 and 6.5 μmol m^{-3} s^{-1} for the burned and unburned ponds, respectively. Parameters were not explicitly calibrated to match O_2 concentrations, as modeled concentrations aligned in magnitude with observations after calibration to match CH_4 and CO_2 concentrations.

Figures 3c and 3d compare the modeled and observed CO_2 concentrations in the two ponds at a depth of 1 m. The model matches the pattern of the measured CO_2 signal, with MAEs of 15.4 and 8.1 μM, and R2s of 0.69 and 0.42 for the unburned and burned ponds, respectively. Since only a few discrete measurements were available for CH_4 and O_2 concentrations, we plot them in the form of the box plot comparison, where the seven water samples available over July–September 2022 are shown in Figure 4. For the unburned pond, one sample yielded a CH_4 concentration of 44.18 μM. This measurement was disregarded in Figure 4 and Table 2 because it would have

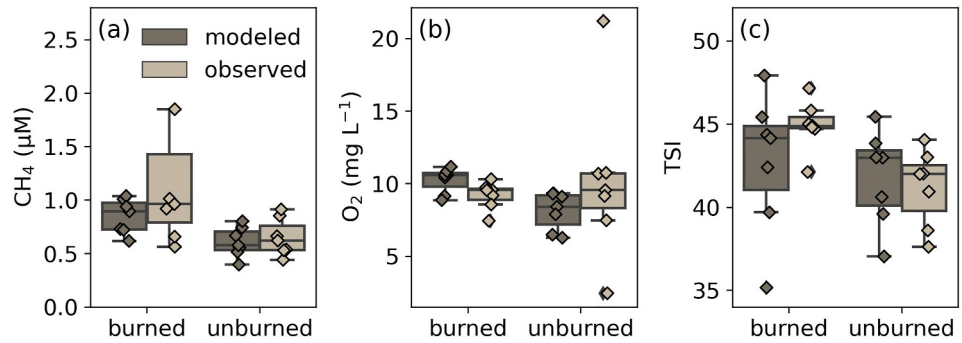

Figure 4. Box plots of modeled and observed (a) CH_4 concentrations, (b) O_2 concentrations, and (c) trophic state index (TSI) for the burned and unburned ponds in the YKD. Concentration measurements were taken from water samples collected at discrete points in time during summer 2022 at a 1 m depth. Burned pond samples were collected on July 9, 17, and 24, August 19 and 27, and September 2 and 8. Unburned pond samples were collected on July 3, 11, and 22, August 15, 22, and 28, and September 5.

skewed the statistics given the low sample size although similarly high CH_4 concentrations have been observed (Bastviken et al., 2008).

The MAEs between measured and modeled CH_4 concentrations were 0.33 and 0.2 μM for the burned and unburned ponds, correspondingly. The MAEs between measured and modeled O_2 concentrations were 6.5 and 0.73 mg L^{-1} for the unburned and burned ponds, correspondingly. The high MAE of modeled O_2 concentrations in the unburned pond was due to the considerable variability in two measured concentrations. However, the distributions of O_2 concentrations show a reasonable alignment (Figure 4b). The comparison metrics are documented in Table 2.

3.1.3. Primary Productivity

Average modeled TSI on the observation dates was 39.2 for both ponds, compared with observed TSI of 44.0 and 39.0 for the burned and unburned ponds respectively (Figure 4c). Overall, modeled and observed TSI had better agreement at the unburned pond (MAE: 1.3) compared with the burned pond (MAE: 5.0). Observed TSI had lower temporal variability at the burned pond than the unburned pond, whereas modeled TSI variability was higher at the burned pond. Overall, modeled TSI variability was greater than observed, but both are characteristic of slightly mesotrophic ponds (Carlson, 1996).

Table 2
Statistics on the Model-Data Comparisons and Sensitivity Analysis Runs for No-Snow Conditions (NS), 20% Increase in Downward Shortwave Radiation (SW20), and 1% (2.7°C) Increase in Air Temperature (TA1)

		Base case			NS	SW20	TA1
Pond		Mean (SD)	MAE	R^2	Mean (SD)	Mean (SD)	Mean (SD)
Burned	Twater (°C)	7.7 (5.4)	1.24	0.52	7.8 (5.4)	8.3 (5.9)	8.3 (5.7)
	CO2 (uM)	38.7 (5.4)	8.01	0.42	38.2 (5.4)	38.7 (5.7)	38.2 (5.0)
	CH4 (uM)	0.94 (0.6)	0.33	–	0.96 (1.4)	0.90 (0.7)	0.87 (0.4)
	DO (mg L^{-1})	10.7 (1.3)	0.73	–	10.9 (1.4)	10.6 (1.5)	10.7 (1.4)
Unburned	Twater (°C)	7.8 (5.2)	1.06	0.82	8.0 (5.1)	8.4 (5.7)	8.4 (5.4)
	CO2 (uM)	97.6 (17.6)	15.37	0.69	96.1 (18.4)	99.4 (19.7)	99.3 (21.5)
	CH4 (uM)	1.2 (2.2)	0.2	–	1.1 (1.8)	1.3 (3.6)	2.5 (10.0)
	DO (mg L^{-1})	8.7 (1.8)	6.47	–	8.8 (1.8)	8.4 (1.9)	8.5 (1.8)

Note. Means and standard deviations for each value were calculated over the ice-free season during final year of simulation at the pond bottom. Mean absolute error (MAE) and Coefficients of Determination (R^2) between modeled and observed concentrations were calculated for the base case. R^2 was only calculated for water temperature and CO_2 concentrations because these variables were continuously observed.

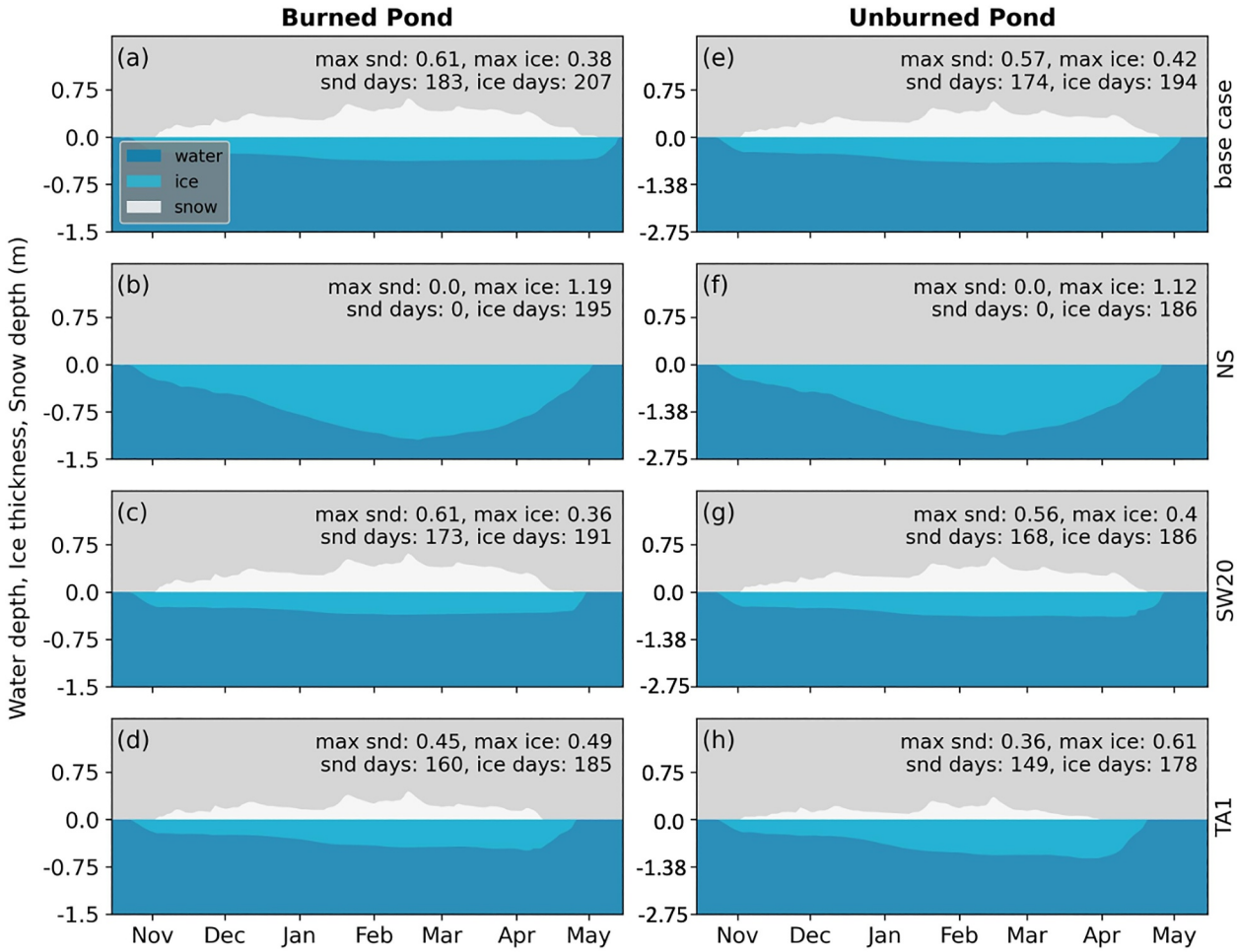

Figure 5. The plots of snow and ice thickness modeled at the burned pond (a–d) and unburned pond (e–h) in the Yukon–Kuskokwim Delta for base case (first row), no snow (NS; second row), 20% shortwave downward radiation increase (SW20; third row), and 1% (2.7°C) air temperature increase (TA1; fourth row).

3.2. Model Sensitivity to Meteorological Inputs

3.2.1. Snow and Ice Cover

We compared the outcomes of three different experiments (i.e., NS, SW20, and TA1) with the base case, where input meteorology was not altered. These input sensitivity analyses identified the complex interplay between temperature, radiation, and snow conditions in determining the duration and physical properties of ice and snow cover on ponds, with implications for understanding the impacts of climate change on these ecosystems.

Between the two ponds, the burned pond had longer ice durations for all climate experiments (Figure 5), likely due to its smaller volume and surface area. The base case experiment resulted in the longest duration of snow and ice cover across the ponds. The NS experiment led to the formation of the thickest ice among all the cases. However, this thick ice melted more rapidly compared to the ice formed under the base case and SW20. Ice and snow layers in SW20 were very similar to the base case during the snow accumulation phase (Nov. - mid March), but both ice and snow melted more rapidly during snow ablation (mid-March–April). The TA1 experiment resulted in the shortest duration of snow and ice cover, however, ice thickness was the second greatest after NS. Increasing air temperature by 2.7°C resulted in a 13% and 14% decrease in snow cover duration for the burned and unburned ponds, and a 10% and 8% decrease in ice cover duration, respectively.

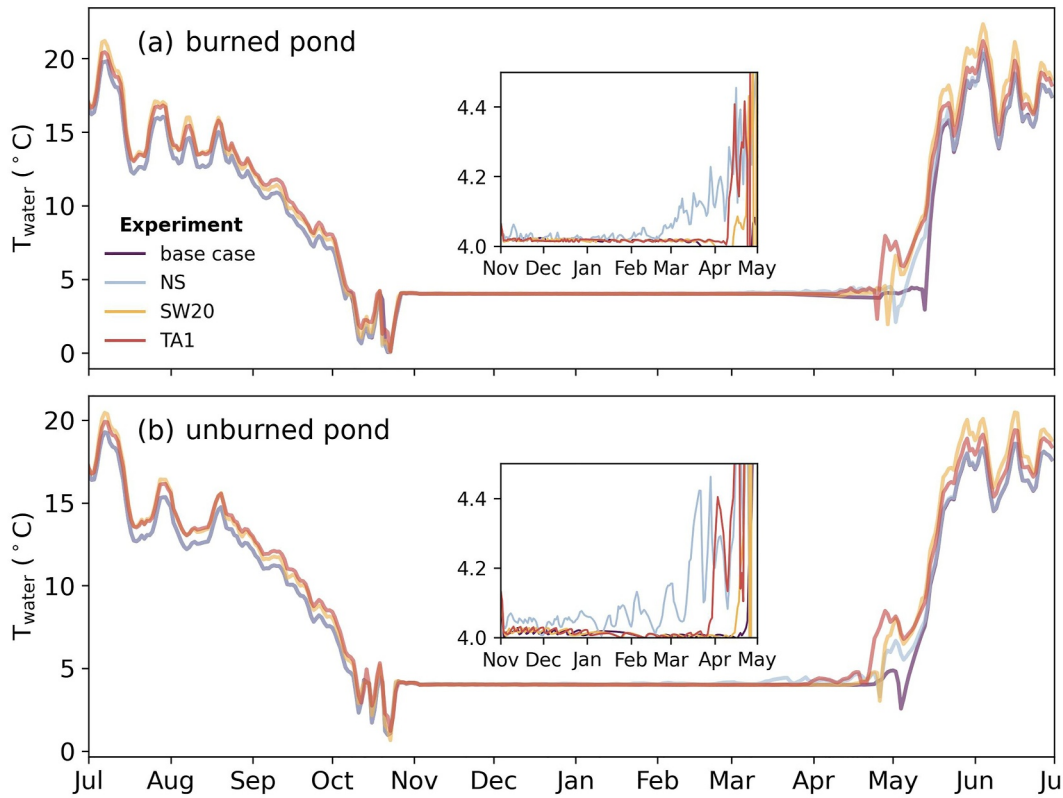

Figure 6. The daily times series of water temperatures at depth (burned: 1.4 m; unburned: 2.5 m) modeled at the (a) burned (b) unburned ponds at Yukon–Kuskokwim Delta for the base case (purple), no snow (blue; NS), 20% shortwave downward radiation increase (yellow; SW20), and 1% (2.7°C) air temperature increase (red; TA1). Water temperatures for the base case and no-snow experiments overlap for most of the year except for April and May. Inlay plots show the same water temperature data with enhanced *x* and *y*-axes.

3.2.2. Water Temperature

Figure 6 presents variations in water temperatures at depth (burned: 1.4 m; unburned: 2.5 m) under different climate experiments. The water temperatures at depth were the same for all simulations except for NS under ice cover (Figure 6), when the water was inversely stratified (Figure S3 in Supporting Information S1). For the NS simulation, water temperatures were slightly higher under ice (Figure 6) than any other experiment and showed weaker inverse stratification than the base case (Figure S3 in Supporting Information S1). NS water temperatures increased prior to ice melt due to increasing penetration of radiation through the ice. Ice cover in NS melted out slightly before the base case experiment, and water temperatures warmed correspondingly. After the spring melt, NS water temperatures quickly assimilated into the base case experiment. Compared to the base case, the TA1 experiment resulted in an average water temperature increase of 0.6°C in the unburned and burned ponds during the ice-free season. The greatest increases in water temperatures relative to the base case occurred in April and May. Water temperatures in SW20 were 0.6°C higher during the ice-free season in the unburned and burned ponds as compared with the base case. Warming under increased shortwave radiation (SW20) was high during May due to earlier ice-melt, with pronounced warming, above TA1, during the summer.

3.2.3. CO_2, O_2, and CH_4 Concentrations

Simulated CH_4 concentrations exhibited a similar behavior across all four evaluated experiments during the ice-free period. Under ice cover, the base case had the highest CH_4 concentrations at depth, followed by the TA1 and SW20 simulations, and the NS simulation had the lowest concentrations (Figures 7a and 7d). The rate of increase in CH_4 concentrations under ice cover was similar for the base case, TA1, and SW20 simulations, and was slightly lower for the NS simulation. The timing and magnitudes of peak CH_4 concentrations were determined by the duration of ice cover.

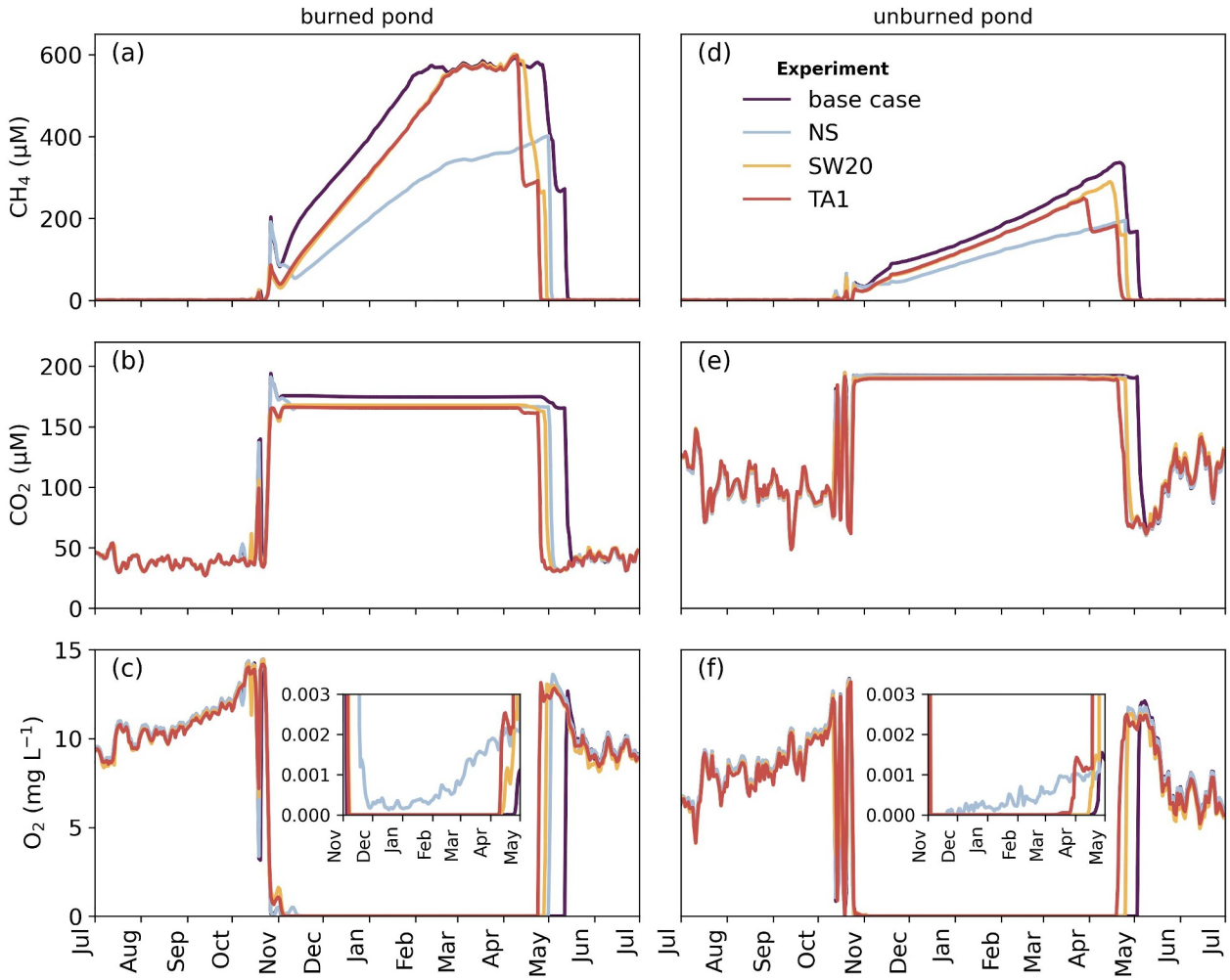

Figure 7. Concentrations of methane, carbon dioxide, and oxygen at depth (burned: 1.4 m; unburned: 2.5 m) for the burned (a–c) and unburned (d–f) ponds. Plots (c) and (f) contain inlays of the same O_2 concentration data with an enhanced *y*-axis. Different experiments are shown with different colors.

The simulations reveal distinctions in CO_2 concentrations, with no to minor differences observed up to the point of initial ice formation and throughout the duration of ice coverage (Figures 7b and 7e). The divergence in CO_2 concentrations becomes pronounced subsequent to the ice melt phase. For both ponds, all experiments exhibited a pattern characterized by a sudden increase in CO_2 concentration during ice formation and abruptly declined after ice melt. The average CO_2 concentration prior- and post-ice melt was around 39 μM in the burned pond. The unburned pond exhibited more dynamic CO_2 concentration, with the mean around 100 μM during the ice-free period.

The simulations of O_2 concentrations showed a gradual increase from July until ice formation in late October and decreased post-ice through June (Figures 7c and 7f). During the ice season, both ponds were anoxic for all simulations except the NS experiment. In the NS experiment, a small amount of photosynthesis occurred under the ice, allowing for microbial decomposition and CH_4 oxidation.

3.2.4. Fluxes of CO_2, O_2, and CH_4

Cumulative CH_4 fluxes were ~5% higher than the base case for both the SW20 and TA1 experiments for both ponds (Figure 8a). This increase in CH_4 flux was comprised of 90% ebullition and 10% diffusion for SW20, whereas the increase in TA1 was 80% ebullition and 20% diffusion. As compared with the base case, the NS experiment produced ~4% higher cumulative annual CH_4 fluxes. In NS, ebullition accounted for 35% and 50% of the increases in CH_4 fluxes in the burned and unburned ponds, respectively.

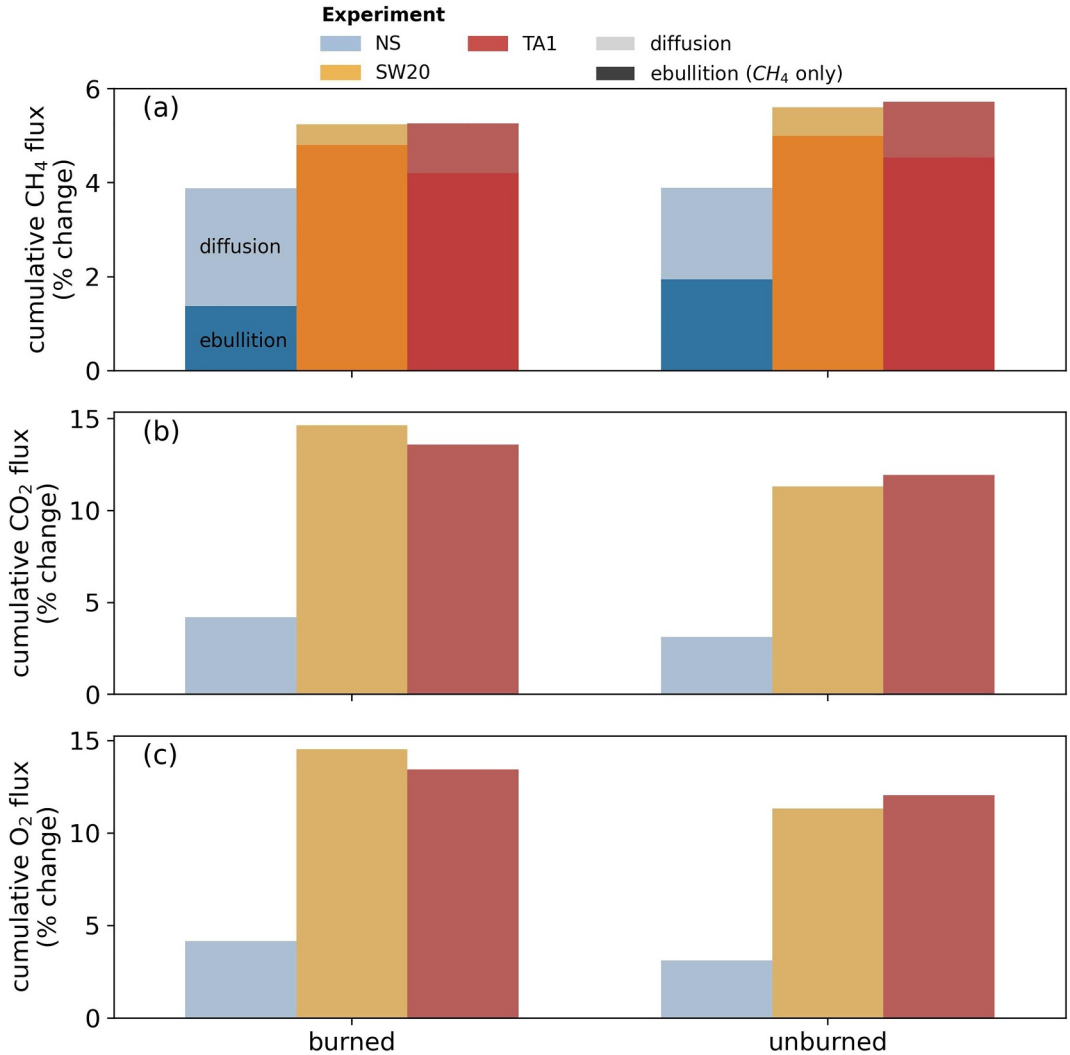

Figure 8. The percent difference between yearly cumulative CH_4 (a), CO_2 (b), and O_2 (c) fluxes for climate experiments (NS, SW20, and TA1) versus the base case at the burned and unburned ponds in the Yukon–Kuskokwim Delta (% change = experiment flux—base case flux). For (a), ebullition and diffusion fluxes are stacked.

CO_2 and O_2 fluxes increased for all experiments (Figures 8b and 8c). For both ponds, the TA1 and SW20 experiments produced the highest increase in CO_2, and O_2 fluxes relative to the base case, followed by the NS experiment. Increases were similar in magnitude for both CO_2 and O_2, and these increases were slightly lower in the unburned pond than the burned pond for any given experiment. Fluxes of CO_2 and O_2 were entirely diffusive. Although the model considers ebullition of these gases (Stepanenko et al., 2016), their ebullition flux was essentially zero.

4. Discussion

Understanding the interconnectedness of climate and lake ecosystems is critical in addressing broader environmental challenges. We conducted numerical simulations using a process-based LAKE model to explore the impact of an increase in air temperature, downward shortwave radiation, and snow cover on the thermal regime of pond waters and their GHG dynamics. Our approach and the results highlight the impact of climate on the Arctic's aquatic ecosystems, emphasizing the role of lake ice in moderating lake thermal and biogeochemical conditions.

4.1. Water Temperature

Biogeochemical processes are intricately coupled with the thermal behavior of the aquatic environment. Consistent with findings by Clark et al. (2022), modeled water temperatures align well with observations (Figures 3a and 3b), requiring no parameter calibration. The subtle disagreement between measured and modeled water temperature at the beginning of the burned pond measurements likely resulted from the time needed for the sensor readings to stabilize in the water.

The ability of the LAKE model to accurately capture the thermal state of these two shallow ponds during ice-free conditions is encouraging for modeling the biogeochemical cycles of these water bodies. As the ponds were completely mixed during summer (Figure S3 in Supporting Information S1), a behavior commonly observed in water bodies of similar size (Holgerson et al., 2022), the model likely provides a reliable representation of the summer temperature profile. During winter, inverse temperature stratification occurs in the model runs, where water temperatures increase with depth (Figure S3 in Supporting Information S1). Weakening of inverse stratification throughout the winter in NS was due to turbulent mixing brought on by continuous penetration of shortwave radiation through the ice, as seen in numerous model and field experiments (Denfeld et al., 2018; Jansen et al., 2019; Wang et al., 2022). Representation of thermal inverse stratification in LAKE under ice cover has been assessed in larger lakes (Stepanenko et al., 2014; Wang et al., 2022), but model performance remains uncertain in smaller ponds. This underscores a need for future research to assess and refine the model's capabilities in under-ice conditions.

4.2. Ice Phenology

The climate experiments highlight the interplay between ice formation, melt, and timing of snowfall. The results show that timing of ice melt is predominantly influenced by the duration of snow cover (Duguay et al., 2003; Preston et al., 2016). However, this relationship varies based on the process driving snow cover change.

In the absence of snow (NS), the ice disappeared earlier than the base case, despite being three times thicker. Notably, the ice did not freeze to the bottom in the NS experiment, even in the shallower burned pond (1.5 m). During the wintertime in 2022, temperatures in the YKD were approximately 1°C colder than the region's 1991–2022 average (NOAA, 2022). Consequently, ponds of similar depth in this region likely do not freeze to the bottom, even in extreme years with low precipitation and air temperatures. In contrast, in colder regions such as the Alaska's North Slope, ponds with depths of 1.3–2.5 m have been found to produce bedfast ice (Arp et al., 2011; Surdu et al., 2014). This highlights the significant influence of regional climate conditions on freeze-thaw dynamics.

Increasing shortwave radiation (SW20) had minimal impact on maximum snow and ice thicknesses and resulted only in a moderate reduction in their duration. This outcome is unsurprising given the low levels of solar radiation during peak snow and ice accumulation in the winter and abrupt increase in solar radiation in the spring. In lower latitudes, however, solar radiation has a much greater influence on the duration of ice cover and wintertime heat balance (Leppäranta & Wen, 2022).

Among the variables tested, increasing air temperature (TA1) had the most prominent effect on ice phenology, consistent with the well-established relationship between air temperature and ice dynamics (Brown & Duguay, 2010). However, the extent of this impact depends on the region's snow climatology. In TA1, snow was much thinner due to temperature spikes in December and February, which led to increased maximum ice thickness due to removal of the insulating snow layer. Despite this, the rapid melting of snow led to the earliest ice disappearance date.

The LAKE model was able to reproduce snow appearance and disappearance dates with a high degree of accuracy despite the snowfall data being sourced from a distant weather station. Given the strong sensitivity of ice duration to snow cover, it is likely that the model provides reasonably accurate estimates of ice duration. However, incorporating more detailed representation of spatiotemporal variability in snow and ice albedo could further improve the model accuracy (Robinson et al., 2021).

4.3. Pond Biogeochemical Calibrations

4.3.1. Calibration of CH_4 Dynamics

During the calibration process, we determined that the parameter R_0 (rate of methane production) exerted the most significant impact on methane concentrations in the model. This aligns with Stepanenko et al. (2016), who also found $K_{hs,CH4}$, the half-saturation constant in CH_4 oxidation, to be a second critical parameter in matching CH_4 concentrations in LAKE. We did not observe the same degree of sensitivity to $K_{hs,CH4}$. This discrepancy likely stems from the fact that we reduced the calibrated maximum oxidation rate (V_{max}) by an order of magnitude compared to (Stepanenko et al., 2016), in order to match CH_4 concentrations that were an order of magnitude higher. We could have achieved a similar match to CH_4 concentrations at higher oxidation rates by increasing R_0 further, but doing so resulted in unrealistically high ebullition rates.

Mean modeled ice-free ebullition rates were 304 and 140 mg m^{-2} d^{-1} for the burned and unburned ponds respectively. These ebullition values are high compared with mean ebullition for small peatland lakes reported in the BAWLD-CH_4 data set (85.6 mg m^{-2} d^{-1}; Kuhn et al., 2021), but still within the data set's observed range. The fraction of produced CH_4 that was oxidized in the ice-free season was 0.01 for the burned pond and 0.04 for the unburned pond. While similarly low fractions have been observed (Cunada et al., 2021), we suspect that our model underestimated oxidation given the observed CH_4 concentrations (Bastviken et al., 2008; Cunada et al., 2021; Knoblauch et al., 2015).

Our omission of groundwater CH_4 influx suggests that the calibration of R_0 and V_{max} compensated for this source to align with measured CH_4 concentrations. Previous studies have found that influx of CH_4 through groundwaters can substantially increase CH_4 diffusion rates and even entirely sustain fluxes of CH_4 from ponds to the atmosphere (Dabrowski et al., 2020; Olid et al., 2022; Paytan et al., 2015). In our study region, Dabrowski et al. (2020) have documented a 200-fold enrichment of CH_4 in groundwater relative to lake water, suggesting that groundwater influx may considerably influence CH_4 concentrations in these ponds.

4.3.2. Calibration of CO_2 Dynamics

The parameter that had the greatest influence on CO_2 concentrations was $\mu_{\beta,0}$, which represents the quantity and quality of organic carbon in sediment available for aerobic decomposition. Similar to R_0, $\mu_{\beta,0}$ needed to be increased to produce moderate correlations between modeled and observed CO_2 concentrations. This adjustment likely compensated for the significantly lower average DOC values in the model (0.0009 mg L^{-1} for burned, 0.0003 mg L^{-1} for unburned) compared with measurements (17.2 mg L^{-1} for burned, 11.9 mg L^{-1} for unburned). This discrepancy indicates that a substantial portion of DOC is delivered to these ponds from the terrestrial subsurface. Influx of DOC has been shown to significantly contribute to CO_2 production in high-latitude ponds (Prėskienis et al., 2024; Saros et al., 2023), but was not accounted for in this study. The only source of DOC in the model runs came from degradation of organic material produced within the ponds, which was clearly not enough to match measurements.

4.3.3. Implications for Model Upscaling

Individual parameters controlling CH_4 production, oxidation, and CO_2 production in the oxygenated sediments required pond-specific calibration to align model outputs with observed gas concentrations. While GHG production rates may vary considerably among lakes of different sizes and eco-climatological regions, water bodies of similar size and in close proximity tend to show similar rates (Knoblauch et al., 2015; Schwefel et al., 2023). Our results indicate that characteristics of the surrounding catchment and subsurface hydrology are also important drivers of GHG fluxes from ponds that must be considered. Future incorporation of lateral transport of chemical and particulate matter may reduce the dependence of model performance on pond-specific calibration and allow for increased confidence in model runs over broad spatial domains where in situ data is limited.

4.4. Wildfire-Induced Differences in CO_2 Concentrations

The contrasting CO_2 concentrations observed between the two ponds likely reflect wildfire effects on the surrounding landscape around the ponds. In the YKD, wildfire changed aboveground vegetation community composition (Baillargeon et al., 2022) and surface soil composition (Moubarak et al., 2023), mobilizing soil nutrients and enhancing biogeochemical cycling and downstream export (Zolkos et al., 2022). Post-fire changes

to the vegetation community could also differentially influence herbivory and feces inputs into each pond, promoting the observed differences in CO_2 concentrations (Beard et al., 2023; Kelsey et al., 2016). Sustained amplification of the carbon cycling 7 years post-fire has resulted in increased terrestrial CO_2 uptake, reducing dissolved organic and inorganic carbon inputs into aquatic systems (Ludwig et al., 2022). Ultimately, Zolkos et al. (2022) determined that surrounding watershed characteristics were a more important determinant of biogeochemical variability than burn status. These differences in watershed characteristics were accounted for in the model through calibration of $\mu_{\beta,0}$ which directly controlled the rate of CO_2 production.

4.5. Biogeochemical Response to Climate Experiments

Water temperature, snow cover, and ice disappearance were the primary drivers behind the increased GHG fluxes for each of the climate experiments compared to the base case. Differences in gas concentrations and fluxes were most pronounced during spring and fall, coinciding with ice formation and breakup (Hughes-Allen et al., 2021; Xue et al., 2024).

4.5.1. CH_4 Dynamics in Climate Experiments

Increased water temperatures in SW20 and TA1 during spring and summer elevated CH_4 production rates due to heating of the soil (Figure S4 in Supporting Information S1), which increased CH_4 emissions primarily through ebullition (Figure 8a). The large increase in ebullition at higher water temperatures can likely be explained by lower CH_4 solubility facilitating bubble formation (Wang et al., 2022). The SW20 and TA1 experiments demonstrated a close coupling between temperature, CH_4 production rates, and CH_4 emission rates, similar to observed in Yvon-Durocher et al. (2014). In reality, other factors such as primary productivity and CH_4 oxidation can greatly alter the temperature dependance of cumulative emissions (Bastviken et al., 2002; DelSontro et al., 2016; Knoblauch et al., 2015; Prėskienis et al., 2021). In the LAKE simulations, organic substrate was not coupled with changes in productivity, rather the substrate quality and quantity were calibrated by proxy with the static R_0 parameter. In the model experiments, CH_4 oxidation rates were calibrated too low to have a prominent impact on modeled emissions.

The NS experiment revealed a distinct pathway for increased CH_4 emissions under reduced winter precipitation. Cumulative CH_4 emissions rose ~4% driven largely by diffusive emissions, the increase of which was entirely due to the ice-melt diffusion pulse (Figures S5a and S5b in Supporting Information S1). This pulse, which has been widely observed to be a significant portion of the CH_4 emission budget (Karlsson et al., 2013; Phelps et al., 1998), was 43% and 25% higher than the base case for the burned and unburned ponds, respectively. Surprisingly, under-ice ebullition was also highest in the NS experiment (Figures S5c and S5d in Supporting Information S1). While NS slightly increased CH_4 production above the base case due to elevated soil surface temperatures (Figure S4 in Supporting Information S1), production was still lower than SW20 and TA1 (Figures S5e and S5f in Supporting Information S1). More importantly, higher soil surface temperatures lowered CH_4 solubility at the soil surface where bubbles are released in the model (Stepanenko et al., 2016). A portion of these bubbles escaped into the atmosphere, but some were trapped under the ice and diffused into the water over time (McGinnis et al., 2006; Stepanenko et al., 2016), leading to higher CH_4 concentrations at the water surface (Figures S5g and S5h in Supporting Information S1).

Penetration of shortwave radiation also led to elevated photosynthesis (Figures S6a and S6b in Supporting Information S1), O_2 concentrations (Figures 7c and 7f) and CH_4 oxidation (Figures S6c and S6d in Supporting Information S1) beneath the ice in NS, which commonly occurs in winter under low-snow conditions (Jansen et al., 2021). Oxidation reduced CH_4 concentrations at depth (Figures S6c and S6d in Supporting Information S1; Figures 7a and 7d), however surface concentrations remained high due to bubble dissolution (Figures S5g and S5h in Supporting Information S1). This below-ice chain of events catalyzed by shortwave penetration occurred briefly in the other three experiments, noted by an initial abrupt dip in CH_4 concentrations after snow disappearance but preceding ice disappearance (Figures 7a and 7d).

Penetration of solar radiation through ice cover and its impacts on lake temperatures and mixing regime has been observed and modeled in previously on lakes with low snow coverage and in late winter (Jansen et al., 2021; Wang et al., 2022), but the impacts on biogeochemistry and GHG concentrations are understudied (Denfeld et al., 2018). Under-ice photosynthesis, methanogenesis, and oxidation have been observed in the field (Bramburger et al., 2023; Crevecoeur et al., 2017; Elder et al., 2019). In a snow-removal experiment, (Garcia

et al., 2019) found that enhanced shortwave penetration led to greater abundance of heterotrophic bacteria and higher CH_4 concentrations, however, specific drivers were not determined. Increased CH_4 surface concentrations in NS were only partially explained by methanogenic productivity. This model experiment indicated that CH_4 solubility at the water-sediment interface had a more dominant influence on CH_4 dynamics in no-snow conditions under ice. However, there are likely additional processes that were not identified and require further investigation. The importance of this process in terms of overall GHG budgets remains uncertain due to the potential rarity of significant light penetration throughout an extended period in winter (Huang et al., 2021; Kirillin et al., 2012). Other processes like influx terrestrial snowmelt may exert a more dominant influence in observed springtime fluxes (Jansen et al., 2019).

4.5.2. CO_2 Dynamics in Climate Experiments

Increases in CO_2 emissions were a result of increases in CO_2 production due to elevated water temperatures and earlier ice melt. Elevated summertime sediment temperatures in TA1 and SW20 resulted in the highest modeled CO_2 production in the sediment and consequent emission (Figures S4 and S7 in Supporting Information S1) for SW20 followed by TA1. Photosynthesis also increased during the summer months (Figure S7 in Supporting Information S1) in TA1 and SW20, however, the increase was not enough to offset the increases in biochemical CO_2 production, similar to findings from controlled experiments (Staehr & Sand-Jensen, 2006). Earlier ice disappearance was of equal importance for increasing CO_2 emissions in TA1 and SW20, and the primary cause in NS. Faster ice melt allowed for an earlier start to primary production and CO_2 production through sedimentary oxygen demand (Figure S7 in Supporting Information S1). The experiments confirm similar findings from (Jansen et al., 2019) that oxygen availability exerts the primary control on CO_2 production and flux during winter and immediately after ice disappearance. However, (Jansen et al., 2019) did not find strong correlations between water temperature and CO_2 flux during the warm season due to the dominance of DOC influx as a driver of warm season CO_2 emissions.

4.6. Implications of Climate Change

Under rapidly warming conditions, GHG cycling in high-latitude water bodies is expected to undergo significant changes. Recent lake phenological records indicate the duration of ice cover is shrinking at a rate of one day per year (Sharma et al., 2021). Ponds that may have historically frozen to the bottom will produce bedfast ice less frequently, crossing a critical threshold (Arp et al., 2012, 2016), as continuous exposure of soil to unfrozen water will promote talik development and GHG emissions (Arp et al., 2016). Our findings indicate that shorter ice duration and higher water temperatures drive increased GHG emissions.

There are several processes that this work did not account for that could either enhance or mitigate some of the observed model responses to climatic drivers. Productivity of aquatic vegetation was not included in our simulations due to its absence in the study ponds. Rehder et al. (2023) found that growth of vascular aquatic vegetation under a range of climate scenarios was a primary driver of enhanced CH_4 emissions through plant-mediated ebullition. Our omission of plant-mediated gas flux may underestimate total GHG fluxes from these ponds, although the presence of vascular plants was minimal in the study ponds.

It is likely that some of the anticipated increases in CH_4 emissions could partially be offset by increases in CH_4 oxidation. Our model simulations did not consider the potential temperature dependance of oxidation. Some have identified this dependance to be low (Duc et al., 2010), but others have found its inclusion to improve model comparisons with field data (Tan et al., 2024). The LAKE model also does not implement anaerobic CH_4 oxidation, a process that may become more prominent in high-latitudes due to changes in the nature of DOC fluxes into water bodies brought on by permafrost thaw (Kurek et al., 2023). Influx for DOC and other forms of carbon are anticipated to increase with permafrost thaw, which could enhance CO_2 and CH_4 fluxes (Vonk et al., 2015).

Permafrost thaw-driven changes to hydrology such as lake creation, lake drainage, and alteration of subsurface flows can profoundly impact GHG cycles in high latitudes and are important processes to consider in future projections of GHG emissions (Gao et al., 2013; Tan & Zhuang, 2015b; Van Huissteden et al., 2011), but were out of the scope of this work.

Lastly, GHG production in ponds has been linked with other important biogeochemical processes that could be enhanced under a warming climate (e.g., mercury methylation) (Kelly et al., 1997). Further refinement of similar modeling approaches could lend itself to a more comprehensive understanding of other aquatic processes that are pertinent to the ecosystem services provided by high-latitude water bodies.

5. Conclusions

We utilized the LAKE numerical model to assess the impacts of climatic drivers on CO_2, CH_4, and O_2 concentrations and fluxes in two tundra ponds. The study emphasizes the complex and sensitive nature of biogeochemical processes in Arctic ponds to small changes in water temperature and ice cover duration. The results underline the importance of field measurements and model parameter calibration for representing aquatic ecosystem processes.

Our research indicates that a 20% rise in shortwave radiation or a 2.7°C uptick in air temperatures could result in a 5% increase in CH_4 fluxes and an over 10% increase in CO_2 fluxes. With the Arctic warming more rapidly than lower latitudes (Ballinger et al., 2024; Constable et al., 2022), predictions have the Arctic warming between 3.3°C and 10°C by 2100 (AMAP, 2021). Should this warming occur linearly, we could see up to a threefold surge in our initial CH_4 and CO_2 flux estimates, to 12%–15% and 12%–36%, respectively. Additionally, experiments without snow revealed a 4% rise in CH_4 and CO_2 fluxes, demonstrating that lower water temperatures do not necessarily diminish fluxes. The ice season's length, particularly the ice melt phase, plays a crucial role in elevating cumulative GHG fluxes. Nonetheless, the timing of ice melt is not the only contributor to increased fluxes; other factors such as groundwater influx and aquatic vegetation also play a significant role (Olid et al., 2022; Rehder et al., 2023). The effects of groundwater influx and vegetation need further investigation, which falls outside the purview of our current study.

Data Availability Statement

Raw and processed eddy covariance data has been submitted to the Ameriflux Network for the unburned (US-YK2) and burned (US-YK1) towers. Pond gas concentrations and biogeochemical data can be found on the Arctic Data Center (Hung et al., 2024). The LAKE model version used, along with input data and configuration files can be found at Mullen, Jafarov, and Gurbanov (2025). The output data and scripts for preprocessing, post-processing, visualization, and analysis can be found at Mullen, Jafarov, Gurbanov, and Stepanenko (2025).

Acknowledgments
This work was supported by the National Science Foundation under awards 2211427 and 2211426 to EEJ and BAP, respectively. Field research and eddy covariance tower funding was provided by the Gordon and Betty Moore Foundation (Grant 8414) to SMN and BMR. VS was supported by Russian Ministry of Science and Higher Education (agreement 075-15-2022-284). We also thank the JAMES editor, associate editor, and three reviewers whose feedback contributed greatly to the quality of this paper.

References

Abbott, B. W., Jones, J. B., Schuur, E. A. G., Chapin Iii, F. S., Bowden, W. B., Bret-Harte, M. S., et al. (2016). Biomass offsets little or none of permafrost carbon release from soils, streams, and wildfire: An expert assessment. *Environmental Research Letters*, *11*(3), 034014. https://doi.org/10.1088/1748-9326/11/3/034014

Abnizova, A., Siemens, J., Langer, M., & Boike, J. (2012). Small ponds with major impact: The relevance of ponds and lakes in permafrost landscapes to carbon dioxide emissions. *Global Biogeochemical Cycles*, *26*(2), 2011GB004237. https://doi.org/10.1029/2011GB004237

Aizaki, M., Otsuki, A., Fukushima, T., Hosomi, M., & Muraoka, K. (1981). Application of Carlson's trophic state index to Japanese lakes and relationships between the index and other parameters: With 2 figures and 4 tables in the text. *SIL Proceedings, 1922-2010*, *21*(1), 675–681. https://doi.org/10.1080/03680770.1980.11897067

AMAP. (2021). AMAP Arctic climate change update 2021: Key trends and impacts. *Arctic Monitoring and Assessment Programme (AMAP)*, *21*, 148.

Arp, C. D., Jones, B. M., Engram, M., Alexeev, V. A., Cai, L., Parsekian, A., et al. (2018). Contrasting lake ice responses to winter climate indicate future variability and trends on the Alaskan Arctic Coastal Plain. *Environmental Research Letters*, *13*(12), 125001. https://doi.org/10.1088/1748-9326/aae994

Arp, C. D., Jones, B. M., Grosse, G., Bondurant, A. C., Romanovsky, V. E., Hinkel, K. M., & Parsekian, A. D. (2016). Threshold sensitivity of shallow Arctic lakes and sublake permafrost to changing winter climate. *Geophysical Research Letters*, *43*(12), 6358–6365. https://doi.org/10.1002/2016GL068506

Arp, C. D., Jones, B. M., Lu, Z., & Whitman, M. S. (2012). Shifting balance of thermokarst lake ice regimes across the Arctic Coastal Plain of northern Alaska. *Geophysical Research Letters*, *39*(16), 2012GL052518. https://doi.org/10.1029/2012GL052518

Arp, C. D., Jones, B. M., Urban, F. E., & Grosse, G. (2011). Hydrogeomorphic processes of thermokarst lakes with grounded-ice and floating-ice regimes on the Arctic coastal plain, Alaska. *Hydrological Processes*, *25*(15), 2422–2438. https://doi.org/10.1002/hyp.8019

Baillargeon, N., Pold, G., Natali, S. M., & Sistla, S. A. (2022). Lowland tundra plant stoichiometry is somewhat resilient decades following fire despite substantial and sustained shifts in community structure. *Arctic Antarctic and Alpine Research*, *54*(1), 525–536. https://doi.org/10.1080/15230430.2022.2121246

Ballinger, T. J., Crawford, A., & Serreze, M. C. (2024). NOAA Arctic report card 2024: Surface air temperature. https://doi.org/10.25923/MJHX-3J40

Bastviken, D., Cole, J. J., Pace, M. L., & Van De Bogert, M. C. (2008). Fates of methane from different lake habitats: Connecting whole-lake budgets and CH_4 emissions. *Journal of Geophysical Research*, *113*(G2), 2007JG000608. https://doi.org/10.1029/2007JG000608

Bastviken, D., Ejlertsson, J., & Tranvik, L. (2002). Measurement of methane oxidation in lakes: A comparison of methods. *Environmental Science & Technology*, *36*(15), 3354–3361. https://doi.org/10.1021/es010311p

Beard, K. H., Kelsey, K. C., Choi, R. T., Welker, J. M., & Leffler, A. J. (2023). Goose feces effects on subarctic soil nitrogen availability and greenhouse gas fluxes. *Ecosystems*, *26*(1), 187–200. https://doi.org/10.1007/s10021-022-00752-x

Beckebanze, L., Rehder, Z., Holl, D., Wille, C., Mirbach, C., & Kutzbach, L. (2022). Ignoring carbon emissions from thermokarst ponds results in overestimation of tundra net carbon uptake. *Biogeosciences*, *19*(4), 1225–1244. https://doi.org/10.5194/bg-19-1225-2022

Bramburger, A. J., Ozersky, T., Silsbe, G. M., Crawford, C. J., Olmanson, L. G., & Shchapov, K. (2023). The not-so-dead of winter: Underwater light climate and primary productivity under snow and ice cover in inland lakes. *Inland Waters*, *13*(1), 1–12. https://doi.org/10.1080/20442041.2022.2102870

Brown, L. C., & Duguay, C. R. (2010). The response and role of ice cover in lake-climate interactions. *Progress in Physical Geography: Earth and Environment*, *34*(5), 671–704. https://doi.org/10.1177/0309133310375653

Carlson, R. E. (1977). A trophic state index for lakes. *Limnology & Oceanography*, *22*(2), 361–369. https://doi.org/10.4319/lo.1977.22.2.0361

Carlson, R. E. (1996). *A coordinator's guide to volunteer lake monitoring methods* (Vol. 96, p. 305). North American Lake Management Society.

Clark, J. A., Jafarov, E. E., Tape, K. D., Jones, B. M., & Stepanenko, V. (2022). Thermal modeling of three lakes within the continuous permafrost zone in Alaska using the LAKE 2.0 model. *Geoscientific Model Development*, *15*(19), 7421–7448. https://doi.org/10.5194/gmd-15-7421-2022

Constable, A. J., Harper, S., Dawson, J., Holsman, K., Mustonen, T., Piepenburg, D., & Rost, B. (2022). Cross chapter paper 6: Polar regions. In H.-O. Pörtner, D. C. Roberts, M. Tignor, E. S. Poloczanska, K. Mintenbeck, A. Alegría, et al. (Eds.), *Climate change 2022: Impacts, adaptation and vulnerability. Contribution of working group II to the sixth assessment report of the intergovernmental panel on climate change* (pp. 2319–2368). Cambridge University Press. https://doi.org/10.1017/9781009325844.023

Crevecoeur, S., Vincent, W. F., Comte, J., Matveev, A., & Lovejoy, C. (2017). Diversity and potential activity of methanotrophs in high methane-emitting permafrost thaw ponds. *PLoS One*, *12*(11), e0188223. https://doi.org/10.1371/journal.pone.0188223

Cunada, C. L., Lesack, L. F. W., & Tank, S. E. (2021). Methane emission dynamics among CO2-absorbing and thermokarst lakes of a great Arctic delta. *Biogeochemistry*, *156*(3), 375–399. https://doi.org/10.1007/s10533-021-00853-0

Dabrowski, J. S., Charette, M. A., Mann, P. J., Ludwig, S. M., Natali, S. M., Holmes, R. M., et al. (2020). Using radon to quantify groundwater discharge and methane fluxes to a shallow, tundra lake on the Yukon-Kuskokwim Delta, Alaska. *Biogeochemistry*, *148*(1), 69–89. https://doi.org/10.1007/s10533-020-00647-w

DelSontro, T., Boutet, L., St-Pierre, A., Del Giorgio, P. A., & Prairie, Y. T. (2016). Methane ebullition and diffusion from northern ponds and lakes regulated by the interaction between temperature and system productivity. *Limnology & Oceanography*, *61*(S1), S62–S77. https://doi.org/10.1002/lno.10335

Denfeld, B. A., Baulch, H. M., Del Giorgio, P. A., Hampton, S. E., & Karlsson, J. (2018). A synthesis of carbon dioxide and methane dynamics during the ice-covered period of northern lakes. *Limnology and Oceanography Letters*, *3*(3), 117–131. https://doi.org/10.1002/lol2.10079

Dissing, D., & Wendler, G. (1998). Solar radiation climatology of Alaska. *Theoretical and Applied Climatology*, *61*(3–4), 161–175. https://doi.org/10.1007/s007040050061

Duc, N. T., Crill, P., & Bastviken, D. (2010). Implications of temperature and sediment characteristics on methane formation and oxidation in lake sediments. *Biogeochemistry*, *100*(1–3), 185–196. https://doi.org/10.1007/s10533-010-9415-8

Duguay, C. R., Flato, G. M., Jeffries, M. O., Ménard, P., Morris, K., & Rouse, W. R. (2003). Ice-cover variability on shallow lakes at high latitudes: Model simulations and observations. *Hydrological Processes*, *17*(17), 3465–3483. https://doi.org/10.1002/hyp.1394

Elder, C. D., Schweiger, M., Lam, B., Crook, E. D., Xu, X., Walker, J., et al. (2019). Seasonal sources of whole-lake CH_4 and CO_2 emissions from interior Alaskan thermokarst lakes. *Journal of Geophysical Research: Biogeosciences*, *124*(5), 1209–1229. https://doi.org/10.1029/2018JG004735

Elmendorf, S. C., Henry, G. H. R., Hollister, R. D., Björk, R. G., Boulanger-Lapointe, N., Cooper, E. J., et al. (2012). Plot-scale evidence of tundra vegetation change and links to recent summer warming. *Nature Climate Change*, *2*(6), 453–457. https://doi.org/10.1038/nclimate1465

Eugster, W., DelSontro, T., Laundre, J. A., Dobkowski, J., Shaver, G. R., & Kling, G. W. (2022). Effects of long-term climate trends on the methane and CO2 exchange processes of Toolik Lake, Alaska. *Frontiers in Environmental Science*, *10*, 948529. https://doi.org/10.3389/fenvs.2022.948529

Finger Higgens, R. A., Chipman, J. W., Lutz, D. A., Culler, L. E., Virginia, R. A., & Ogden, L. A. (2019). Changing Lake dynamics indicate a drier Arctic in western Greenland. *Journal of Geophysical Research: Biogeosciences*, *124*(4), 870–883. https://doi.org/10.1029/2018JG004879

Frost, G. V., Loehman, R. A., Saperstein, L. B., Macander, M. J., Nelson, P. R., Paradis, D. P., & Natali, S. M. (2020). Multi-decadal patterns of vegetation succession after tundra fire on the Yukon-Kuskokwim Delta, Alaska. *Environmental Research Letters*, *15*(2), 025003. https://doi.org/10.1088/1748-9326/ab5f49

Gao, X., Adam Schlosser, C., Sokolov, A., Anthony, K. W., Zhuang, Q., & Kicklighter, D. (2013). Permafrost degradation and methane: Low risk of biogeochemical climate-warming feedback. *Environmental Research Letters*, *8*(3), 035014. https://doi.org/10.1088/1748-9326/8/3/035014

Garcia, S. L., Szekely, A. J., Bergvall, C., Schattenhofer, M., & Peura, S. (2019). Decreased snow cover stimulates under-ice primary producers but impairs methanotrophic capacity. *Msphere*, *4*(1), 10–1128. https://doi.org/10.1128/mSphere.00626-18

Grant, L., Vanderkelen, I., Gudmundsson, L., Tan, Z., Perroud, M., Stepanenko, V. M., et al. (2021). Attribution of global lake systems change to anthropogenic forcing. *Nature Geoscience*, *14*(11), 849–854. https://doi.org/10.1038/s41561-021-00833-x

Guo, M., Zhuang, Q., Tan, Z., Shurpali, N., Juutinen, S., Kortelainen, P., & Martikainen, P. J. (2020). Rising methane emissions from boreal lakes due to increasing ice-free days. *Environmental Research Letters*, *15*(6), 064008. https://doi.org/10.1088/1748-9326/ab8254

Hatzianastassiou, N., Matsoukas, C., Fotiadi, A., Pavlakis, K. G., Drakakis, E., Hatzidimitriou, D., & Vardavas, I. (2005). Global distribution of Earth's surface shortwave radiation budget. *Atmospheric Chemistry and Physics*, *5*(10), 2847–2867. https://doi.org/10.5194/acp-5-2847-2005

Hesslein, R. H., Rudd, J. W. M., Kelly, C. A., Ramlal, P. S., & Hallard, K. A. (1991). Carbon dioxide pressure in surface waters of Canadian Lakes. Retrieved from https://api.semanticscholar.org/CorpusID:133213811

Holgerson, M. A., Richardson, D. C., Roith, J., Bortolotti, L. E., Finlay, K., Hornbach, D. J., et al. (2022). Classifying mixing regimes in ponds and shallow lakes. *Water Resources Research*, *58*(7), e2022WR032522. https://doi.org/10.1029/2022WR032522

Hu, M., Ma, R., Cao, Z., Xiong, J., & Xue, K. (2021). Remote estimation of trophic state index for inland waters using landsat-8 OLI imagery. *Remote Sensing*, *13*(10), 1988. https://doi.org/10.3390/rs13101988

Huang, W., Zhang, Z., Li, Z., Leppäranta, M., Arvola, L., Song, S., et al. (2021). Under-ice dissolved oxygen and metabolism dynamics in a shallow lake: The critical role of ice and snow. *Water Resources Research*, *57*(5), e2020WR027990. https://doi.org/10.1029/2020WR027990

Hughes-Allen, L., Bouchard, F., Laurion, I., Séjourné, A., Marlin, C., Hatté, C., et al. (2021). Seasonal patterns in greenhouse gas emissions from thermokarst lakes in Central Yakutia (Eastern Siberia). *Limnology & Oceanography*, *66*(S1), S98–S116. https://doi.org/10.1002/lno.11665

Hung, J., Korolev, M., & Natali, S. (2024). *Yukon-Kuskokwim Delta, Alaska unburned and burned aquatic data, 2022*. Arctic Data Center. https://doi.org/10.18739/A2F18SH0T

Jafarov, E. E., Romanovsky, V. E., Genet, H., McGuire, A. D., & Marchenko, S. S. (2013). The effects of fire on the thermal stability of permafrost in lowland and upland black spruce forests of interior Alaska in a changing climate. *Environmental Research Letters*, *8*(3), 035030. https://doi.org/10.1088/1748-9326/8/3/035030

Jammet, M., Dengel, S., Kettner, E., Parmentier, F.-J. W., Wik, M., Crill, P., & Friborg, T. (2017). Year-round CH_4 and CO_2 flux dynamics in two contrasting freshwater ecosystems of the subarctic. *Biogeosciences*, *14*(22), 5189–5216. https://doi.org/10.5194/bg-14-5189-2017

Jansen, J., MacIntyre, S., Barrett, D. C., Chin, Y., Cortés, A., Forrest, A. L., et al. (2021). Winter limnology: How do hydrodynamics and biogeochemistry shape ecosystems under ice? *Journal of Geophysical Research: Biogeosciences*, *126*(6), e2020JG006237. https://doi.org/10.1029/2020JG006237

Jansen, J., Thornton, B. F., Jammet, M. M., Wik, M., Cortés, A., Friborg, T., et al. (2019). Climate-sensitive controls on large spring emissions of CH_4 and CO_2 from northern lakes. *Journal of Geophysical Research: Biogeosciences*, *124*(7), 2379–2399. https://doi.org/10.1029/2019JG005094

Jeffries, M. O., & Morris, K. (2006). Instantaneous daytime conductive heat flow through snow on lake ice in Alaska. *Hydrological Processes*, *20*(4), 803–815. https://doi.org/10.1002/hyp.6116

Jeffries, M. O., Zhang, T., Frey, K., & Kozlenko, N. (1999). Estimating late-winter heat flow to the atmosphere from the lake-dominated Alaskan North Slope. *Journal of Glaciology*, *45*(150), 315–324. https://doi.org/10.3189/002214399793377095

Jensen, T. C., Walseng, B., Hessen, D. O., Dimante-Deimantovica, I., Novichkova, A. A., Chertoprud, E. S., et al. (2019). Changes in trophic state and aquatic communities in high Arctic ponds in response to increasing goose populations. *Freshwater Biology*, *64*(7), 1241–1254. https://doi.org/10.1111/fwb.13299

Johnson, M. S., Matthews, E., Du, J., Genovese, V., & Bastviken, D. (2022). Methane emission from global lakes: New spatiotemporal data and observation-driven modeling of methane dynamics indicates lower emissions. *Journal of Geophysical Research: Biogeosciences*, *127*(7), e2022JG006793. https://doi.org/10.1029/2022JG006793

Jorgenson, M. T., & Shur, Y. (2007). Evolution of lakes and basins in northern Alaska and discussion of the thaw lake cycle. *Journal of Geophysical Research*, *112*(F2), 2006JF000531. https://doi.org/10.1029/2006JF000531

Jorgenson, M. T., Shur, Y. L., & Pullman, E. R. (2006). Abrupt increase in permafrost degradation in Arctic Alaska. *Geophysical Research Letters*, *33*(2), 2005GL024960. https://doi.org/10.1029/2005GL024960

Jorgenson, T., Yoshikawa, K., Kanevskiy, M., Shur, Y., Romanovsky, V., Marchenko, S., et al. (2008). Permafrost characteristics of Alaska - 2008 shapefile [Dataset]. https://catalog.northslopescience.org/dataset/1725

Karlsson, J., Giesler, R., Persson, J., & Lundin, E. (2013). High emission of carbon dioxide and methane during ice thaw in high latitude lakes. *Geophysical Research Letters*, *40*(6), 1123–1127. https://doi.org/10.1002/grl.50152

Kelly, C. A., Rudd, J. W. M., Bodaly, R. A., Roulet, N. P., St.Louis, V. L., Heyes, A., et al. (1997). Increases in fluxes of greenhouse gases and methyl mercury following flooding of an experimental reservoir. *Environmental Science & Technology*, *31*(5), 1334–1344. https://doi.org/10.1021/es9604931

Kelsey, K. C., Leffler, A. J., Beard, K. H., Schmutz, J. A., Choi, R. T., & Welker, J. M. (2016). Interactions among vegetation, climate, and herbivory control greenhouse gas fluxes in a subarctic coastal wetland. *Journal of Geophysical Research: Biogeosciences*, *121*(12), 2960–2975. https://doi.org/10.1002/2016JG003546

Kirillin, G., Leppäranta, M., Terzhevik, A., Granin, N., Bernhardt, J., Engelhardt, C., et al. (2012). Physics of seasonally ice-covered lakes: A review. *Aquatic Sciences*, *74*(4), 659–682. https://doi.org/10.1007/s00027-012-0279-y

Knoblauch, C., Spott, O., Evgrafova, S., Kutzbach, L., & Pfeiffer, E. (2015). Regulation of methane production, oxidation, and emission by vascular plants and bryophytes in ponds of the northeast Siberian polygonal tundra. *Journal of Geophysical Research: Biogeosciences*, *120*(12), 2525–2541. https://doi.org/10.1002/2015JG003053

Koehler, B., Landelius, T., Weyhenmeyer, G. A., Machida, N., & Tranvik, L. J. (2014). Sunlight-induced carbon dioxide emissions from inland waters. *Global Biogeochemical Cycles*, *28*(7), 696–711. https://doi.org/10.1002/2014GB004850

Kratzer, C. R., & Brezonik, P. L. (1981). A carlson-type trophic state index for nitrogen in Florida Lakes. *JAWRA Journal of the American Water Resources Association*, *17*(4), 713–715. https://doi.org/10.1111/j.1752-1688.1981.tb01282.x

Kuhn, M. A., Varner, R. K., Bastviken, D., Crill, P., MacIntyre, S., Turetsky, M., et al. (2021). BAWLD-CH_4: A comprehensive dataset of methane fluxes from boreal and arctic ecosystems. *Earth System Science Data*, *13*(11), 5151–5189. https://doi.org/10.5194/essd-13-5151-2021

Kurek, M. R., Garcia-Tigreros, F., Nichols, N. A., Druschel, G. K., Wickland, K. P., Dornblaser, M. M., et al. (2023). High voltage: The molecular properties of redox-active dissolved organic matter in northern high-latitude lakes. *Environmental Science & Technology*, *57*(23), 8617–8627. https://doi.org/10.1021/acs.est.3c01782

Kyzivat, E. D., & Smith, L. C. (2023). A closer look at the effects of lake area, aquatic vegetation, and double-counted wetlands on Pan-Arctic Lake methane emissions estimates. *Geophysical Research Letters*, *50*(24), e2023GL104825. https://doi.org/10.1029/2023GL104825

Leppäranta, M., & Wen, L. (2022). Ice phenology in Eurasian lakes over spatial location and altitude. *Water*, *14*(7), 1037. https://doi.org/10.3390/w14071037

Lidstrom, M. E., & Somers, L. (1984). Seasonal study of methane oxidation in Lake Washington. *Applied and Environmental Microbiology*, *47*(6), 1255–1260. https://doi.org/10.1128/aem.47.6.1255-1260.1984

Liikanen, A., Murtoniemi, T., Tanskanen, H., Väisänen, T., & Martikainen, P. J. (2002). Effects of temperature and oxygen availability on greenhouse gas and nutrient dynamics in sediment of a eutrophic mid-boreal lake. *Biogeochemistry*, *59*(3), 269–286. https://doi.org/10.1023/A:1016015526712

Liu, X., & Zhuang, Q. (2023). Methane emissions from arctic landscapes during 2000–2015: An analysis with land and lake biogeochemistry models. *Biogeosciences*, *20*(6), 1181–1193. https://doi.org/10.5194/bg-20-1181-2023

Lofton, D. D., Whalen, S. C., & Hershey, A. E. (2014). Effect of temperature on methane dynamics and evaluation of methane oxidation kinetics in shallow Arctic Alaskan lakes. *Hydrobiologia*, *721*(1), 209–222. https://doi.org/10.1007/s10750-013-1663-x

Lomov, V., Stepanenko, V., Grechushnikova, M., & Repina, I. (2023). Mechanistic modeling of the variability of methane emissions from an artificial reservoir. *Water*, *16*(1), 76. https://doi.org/10.3390/w16010076

Ludwig, S. M., Natali, S. M., Mann, P. J., Schade, J. D., Holmes, R. M., Powell, M., et al. (2022). Using machine learning to predict inland aquatic CO_2 and CH_4 concentrations and the effects of wildfires in the Yukon-Kuskokwim Delta, Alaska. *Global Biogeochemical Cycles*, *36*(4), e2021GB007146. https://doi.org/10.1029/2021GB007146

Ludwig, S. M., Natali, S. M., Schade, J. D., Powell, M., Fiske, G., Schiferl, L. D., & Commane, R. (2023). Scaling waterbody carbon dioxide and methane fluxes in the arctic using an integrated terrestrial-aquatic approach. *Environmental Research Letters*, *18*(6), 064019. https://doi.org/10.1088/1748-9326/acd467

Ludwig, S. M., Schiferl, L., Hung, J., Natali, S. M., & Commane, R. (2024). Resolving heterogeneous fluxes from tundra halves the growing season carbon budget. *Biogeosciences*, *21*(5), 1301–1321. https://doi.org/10.5194/bg-21-1301-2024

Maeda, E. E., Lisboa, F., Kaikkonen, L., Kallio, K., Koponen, S., Brotas, V., & Kuikka, S. (2019). Temporal patterns of phytoplankton phenology across high latitude lakes unveiled by long-term time series of satellite data. *Remote Sensing of Environment*, *221*, 609–620. https://doi.org/10.1016/j.rse.2018.12.006

Matthews, E., Johnson, M. S., Genovese, V., Du, J., & Bastviken, D. (2020). Methane emission from high latitude lakes: Methane-centric lake classification and satellite-driven annual cycle of emissions. *Scientific Reports*, *10*(1), 12465. https://doi.org/10.1038/s41598-020-68246-1

McGinnis, D. F., Greinert, J., Artemov, Y., Beaubien, S. E., & Wüest, A. (2006). Fate of rising methane bubbles in stratified waters: How much methane reaches the atmosphere? *Journal of Geophysical Research*, *111*(C9), 2005JC003183. https://doi.org/10.1029/2005JC003183

Megard, R. O., Tonkyn, D. W., & Senft, W. H. (1984). Kinetics of oxygenic photosynthesis in planktonic algae. *Journal of Plankton Research*, *6*(2), 325–337. https://doi.org/10.1093/plankt/6.2.325

Michaelides, R. J., Schaefer, K., Zebker, H. A., Parsekian, A., Liu, L., Chen, J., et al. (2019). Inference of the impact of wildfire on permafrost and active layer thickness in a discontinuous permafrost region using the remotely sensed active layer thickness (ReSALT) algorithm. *Environmental Research Letters*, *14*(3), 035007. https://doi.org/10.1088/1748-9326/aaf932

Mironov, D., Kourzeneva, E., Ritter, B., & Schneider, N. (2009). Implementation of the lake parameterisation scheme FLake into numerical weather prediction model COSMO. *Boreal Environment Research*, *15*.

Mironov, D. V. (2008). Parameterization of lakes in numerical weather prediction. Description of a Lake Model. In *COSMO technical report* (Vol. 11, p. 44). Offenbach am Main, Germany: German Weather Service. Retrieved from https://api.semanticscholar.org/CorpusID:54696443

Moubarak, M., Sistla, S., Potter, S., Natali, S. M., & Rogers, B. M. (2023). Carbon emissions and radiative forcings from tundra wildfires in the Yukon–Kuskokwim River Delta, Alaska. *Biogeosciences*, *20*(8), 1537–1557. https://doi.org/10.5194/bg-20-1537-2023

Mullen, A., Jafarov, E., & Gurbanov, K. (2025). LAKE model data processing and outputs. *Zenodo*. https://doi.org/10.5281/zenodo.14722247

Mullen, A., Jafarov, E., Gurbanov, K., & Stepanenko, V. (2025). LAKE model used in "modeling thermal and biogeochemical dynamics in two ponds within Alaska's Yukon-Kuskokwim delta: Impacts of climate variability on greenhouse gas fluxes". *Zenodo*. https://doi.org/10.5281/zenodo.14722248

Mullen, A. L., Watts, J. D., Rogers, B. M., Carroll, M. L., Elder, C. D., Noomah, J., et al. (2023). Using high-resolution satellite imagery and deep learning to track dynamic seasonality in small water bodies. *Geophysical Research Letters*, *50*(7), e2022GL102327. https://doi.org/10.1029/2022GL102327

NOAA. (2022). Monthly total precipitation for Bethel Area, AK [Dataset]. https://www.weather.gov/wrh/Climate?wfo=afc

Olid, C., Rodellas, V., Rocher-Ros, G., Garcia-Orellana, J., Diego-Feliu, M., Alorda-Kleinglass, A., et al. (2022). Groundwater discharge as a driver of methane emissions from Arctic lakes. *Nature Communications*, *13*(1), 3667. https://doi.org/10.1038/s41467-022-31219-1

Paytan, A., Lecher, A. L., Dimova, N., Sparrow, K. J., Kodovska, F. G.-T., Murray, J., et al. (2015). Methane transport from the active layer to lakes in the Arctic using Toolik Lake, Alaska, as a case study. *Proceedings of the National Academy of Sciences*, *112*(12), 3636–3640. https://doi.org/10.1073/pnas.1417392112

Phelps, A. R., Peterson, K. M., & Jeffries, M. O. (1998). Methane efflux from high-latitude lakes during spring ice melt. *Journal of Geophysical Research*, *103*(D22), 29029–29036. https://doi.org/10.1029/98JD00044

Pouliot, D., Latifovic, R., & Olthof, I. (2009). Trends in vegetation NDVI from 1 km AVHRR data over Canada for the period 1985–2006. *International Journal of Remote Sensing*, *30*(1), 149–168. https://doi.org/10.1080/01431160802302090

Prėskienis, V., Fortier, D., Douglas, P. M. J., Rautio, M., & Laurion, I. (2024). Permafrost degradation and soil erosion as drivers of greenhouse gas emissions from tundra ponds. *Environmental Research Letters*, *19*(1), 014072. https://doi.org/10.1088/1748-9326/ad1433

Prėskienis, V., Laurion, I., Bouchard, F., Douglas, P. M. J., Billett, M. F., Fortier, D., & Xu, X. (2021). Seasonal patterns in greenhouse gas emissions from lakes and ponds in a High Arctic polygonal landscape. *Limnology & Oceanography*, *66*(S1), S117–S141. https://doi.org/10.1002/lno.11660

Preston, D. L., Caine, N., McKnight, D. M., Williams, M. W., Hell, K., Miller, M. P., et al. (2016). Climate regulates alpine lake ice cover phenology and aquatic ecosystem structure. *Geophysical Research Letters*, *43*(10), 5353–5360. https://doi.org/10.1002/2016GL069036

Ramage, J., Kuhn, M., Virkkala, A., Voigt, C., Marushchak, M. E., Bastos, A., et al. (2024). The net GHG balance and budget of the permafrost region (2000–2020) from ecosystem flux upscaling. *Global Biogeochemical Cycles*, *38*(4), e2023GB007953. https://doi.org/10.1029/2023GB007953

Rantanen, M., Karpechko, A. Y., Lipponen, A., Nordling, K., Hyvärinen, O., Ruosteenoja, K., et al. (2022). The Arctic has warmed nearly four times faster than the globe since 1979. *Communications Earth & Environment*, *3*(1), 168. https://doi.org/10.1038/s43247-022-00498-3

Rehder, Z., Kleinen, T., Kutzbach, L., Stepanenko, V., Langer, M., & Brovkin, V. (2023). Simulated methane emissions from Arctic ponds are highly sensitive to warming. *Biogeosciences*, *20*(14), 2837–2855. https://doi.org/10.5194/bg-20-2837-2023

Riggs, G. A., Hall, D. K., & Román, M. O. (2015). VIIRS snow cover algorithm theoretical basis document (ATBD). Retrieved from https://viirsland.gsfc.nasa.gov/PDF/VIIRS_snow_cover_ATBD_2015.pdf

Robinson, A. L., Ariano, S. S., & Brown, L. C. (2021). The influence of snow and ice albedo towards improved lake ice simulations. *Hydrology*, *8*(1), 11. https://doi.org/10.3390/hydrology8010011

Rosentreter, J. A., Borges, A. V., Deemer, B. R., Holgerson, M. A., Liu, S., Song, C., et al. (2021). Half of global methane emissions come from highly variable aquatic ecosystem sources. *Nature Geoscience*, *14*(4), 225–230. https://doi.org/10.1038/s41561-021-00715-2

Rouse, W. R., Douglas, M. S. V., Hecky, R. E., Hershey, A. E., Kling, G. W., Lesack, L., et al. (1997). Effects of climate change on the freshwaters of Arctic and subarctic North America. *Hydrological Processes*, *11*(8), 873–902. https://doi.org/10.1002/(SICI)1099-1085(19970630)11:8<873::AID-HYP510>3.0.CO;2-6

Rowland, J. C., Travis, B. J., & Wilson, C. J. (2011). The role of advective heat transport in talik development beneath lakes and ponds in discontinuous permafrost: Groundwater flow and lake talik. *Geophysical Research Letters*, *38*(17), L17504. https://doi.org/10.1029/2011GL048497

Sae-Lim, J., Russell, J. M., Vachula, R. S., Holmes, R. M., Mann, P. J., Schade, J. D., & Natali, S. M. (2019). Temperature-controlled tundra fire severity and frequency during the last millennium in the Yukon-Kuskokwim Delta, Alaska. *The Holocene*, *29*(7), 1223–1233. https://doi.org/10.1177/0959683619838036

Saros, J. E., Arp, C. D., Bouchard, F., Comte, J., Couture, R.-M., Dean, J. F., et al. (2023). Sentinel responses of Arctic freshwater systems to climate: Linkages, evidence, and a roadmap for future research. *Arctic Science*, *9*(2), 356–392. https://doi.org/10.1139/as-2022-0021

Saunois, M., Stavert, A. R., Poulter, B., Bousquet, P., Canadell, J. G., Jackson, R. B., et al. (2020). The global methane budget 2000–2017. *Earth System Science Data*, *12*(3), 1561–1623. https://doi.org/10.5194/essd-12-1561-2020

Schwefel, R., MacIntyre, S., Cortés, A., & Sadro, S. (2023). Oxygen depletion and sediment respiration in ice-covered arctic lakes. *Limnology & Oceanography*, *68*(7), 1470–1489. https://doi.org/10.1002/lno.12357

Seekell, D. A., Lapierre, J., Ask, J., Bergström, A., Deininger, A., Rodríguez, P., & Karlsson, J. (2015). The influence of dissolved organic carbon on primary production in northern lakes. *Limnology & Oceanography*, *60*(4), 1276–1285. https://doi.org/10.1002/lno.10096

Sharma, S., Richardson, D. C., Woolway, R. I., Imrit, M. A., Bouffard, D., Blagrave, K., et al. (2021). Loss of ice cover, shifting phenology, and more extreme events in northern hemisphere lakes. *Journal of Geophysical Research: Biogeosciences*, *126*(10), e2021JG006348. https://doi.org/10.1029/2021JG006348

Siebesma, A. P., Soares, P. M. M., & Teixeira, J. (2007). A combined eddy-diffusivity mass-flux approach for the convective boundary layer. *Journal of the Atmospheric Sciences*, *64*(4), 1230–1248. https://doi.org/10.1175/JAS3888.1

Stackpoole, S. M., Butman, D. E., Clow, D. W., Verdin, K. L., Gaglioti, B. V., Genet, H., & Striegl, R. G. (2017). Inland waters and their role in the carbon cycle of Alaska. *Ecological Applications*, *27*(5), 1403–1420. https://doi.org/10.1002/eap.1552

Staehr, P. A., & Sand-Jensen, K. (2006). Seasonal changes in temperature and nutrient control of photosynthesis, respiration and growth of natural phytoplankton communities. *Freshwater Biology*, *51*(2), 249–262. https://doi.org/10.1111/j.1365-2427.2005.01490.x

Stepanenko, V., Mammarella, I., Ojala, A., Miettinen, H., Lykosov, V., & Vesala, T. (2016). LAKE 2.0: A model for temperature, methane, carbon dioxide and oxygen dynamics in lakes. *Geoscientific Model Development*, *9*(5), 1977–2006. https://doi.org/10.5194/gmd-9-1977-2016

Stepanenko, V. M., Jöhnk, K. D., Machulskaya, E., Perroud, M., Subin, Z., Nordbo, A., et al. (2014). Simulation of surface energy fluxes and stratification of a small boreal lake by a set of one-dimensional models. *Tellus A: Dynamic Meteorology and Oceanography*, *66*(1), 21389. https://doi.org/10.3402/tellusa.v66.21389

Stepanenko, V. M., & Lykossov, V. N. (2005). Numerical modeling of heat and moisture transfer processes in a system lake—Soil. *Russian Meteorology and Hydrology*, *3*, 95–104.

Stepanenko, V. M., Valerio, G., & Pilotti, M. (2020). Horizontal pressure gradient parameterization for one-dimensional lake models. *Journal of Advances in Modeling Earth Systems*, *12*(2), e2019MS001906. https://doi.org/10.1029/2019MS001906

Surdu, C. M., Duguay, C. R., Brown, L. C., & Fernández Prieto, D. (2014). Response of ice cover on shallow lakes of the North Slope of Alaska to contemporary climate conditions (1950–2011): Radar remote-sensing and numerical modeling data analysis. *The Cryosphere*, *8*(1), 167–180. https://doi.org/10.5194/tc-8-167-2014

Tan, Z., Yao, H., Melack, J., Grossart, H., Jansen, J., Balathandayuthabani, S., et al. (2024). A lake biogeochemistry model for global methane emissions: Model development, site-level validation, and global applicability. *Journal of Advances in Modeling Earth Systems*, *16*(10), e2024MS004275. https://doi.org/10.1029/2024MS004275

Tan, Z., & Zhuang, Q. (2015a). Arctic lakes are continuous methane sources to the atmosphere under warming conditions. *Environmental Research Letters*, *10*(5), 054016. https://doi.org/10.1088/1748-9326/10/5/054016

Tan, Z., & Zhuang, Q. (2015b). Methane emissions from pan-Arctic lakes during the 21st century: An analysis with process-based models of lake evolution and biogeochemistry. *Journal of Geophysical Research: Biogeosciences*, *120*(12), 2641–2653. https://doi.org/10.1002/2015JG003184

Tan, Z., Zhuang, Q., Shurpali, N. J., Marushchak, M. E., Biasi, C., Eugster, W., & Walter Anthony, K. (2017). Modeling CO_2 emissions from Arctic lakes: Model development and site-level study. *Journal of Advances in Modeling Earth Systems*, *9*(5), 2190–2213. https://doi.org/10.1002/2017MS001028

Tan, Z., Zhuang, Q., & Walter Anthony, K. (2015). Modeling methane emissions from arctic lakes: Model development and site-level study. *Journal of Advances in Modeling Earth Systems*, *7*(2), 459–483. https://doi.org/10.1002/2014MS000344

USDA. (2017). U.S. General soil map (STATSGO2) [Dataset]. https://catalog.data.gov/dataset/u-s-general-soil-map-statsgo2

Van Huissteden, J., Berrittella, C., Parmentier, F. J. W., Mi, Y., Maximov, T. C., & Dolman, A. J. (2011). Methane emissions from permafrost thaw lakes limited by lake drainage. *Nature Climate Change*, *1*(2), 119–123. https://doi.org/10.1038/nclimate1101

Vonk, J. E., Tank, S. E., Bowden, W. B., Laurion, I., Vincent, W. F., Alekseychik, P., et al. (2015). Reviews and syntheses: Effects of permafrost thaw on Arctic aquatic ecosystems. *Biogeosciences*, *12*(23), 7129–7167. https://doi.org/10.5194/bg-12-7129-2015

Walker, R. R., & Snodgrass, W. J. (1986). Model for sediment oxygen demand in lakes. *Journal of Environmental Engineering*, *112*(1), 25–43. https://doi.org/10.1061/(ASCE)0733-9372(1986)112:1(25)

Walter Anthony, K., Schneider von Deimling, T., Nitze, I., Frolking, S., Emond, A., Daanen, R., et al. (2018). 21st-century modeled permafrost carbon emissions accelerated by abrupt thaw beneath lakes. *Nature Communications*, *9*(1), 3262. https://doi.org/10.1038/s41467-018-05738-9

Wang, M., Wen, L., Li, Z., Leppäranta, M., Stepanenko, V., Zhao, Y., et al. (2022). Mechanisms and effects of under-ice warming water in Ngoring Lake of Qinghai–Tibet Plateau. *The Cryosphere*, *16*(9), 3635–3648. https://doi.org/10.5194/tc-16-3635-2022

Watson, A., Stephen, K. D., Nedwell, D. B., & Arah, J. R. M. (1997). Oxidation of methane in peat: Kinetics of CH4 and O2 removal and the role of plant roots. *Soil Biology and Biochemistry*, *29*(8), 1257–1267. https://doi.org/10.1016/S0038-0717(97)00016-3

Wik, M., Varner, R. K., Anthony, K. W., MacIntyre, S., & Bastviken, D. (2016). Climate-sensitive northern lakes and ponds are critical components of methane release. *Nature Geoscience*, *9*(2), 99–105. https://doi.org/10.1038/ngeo2578

Xue, J., Chen, X., Wang, C., Wang, X., & Sun, X. (2024). Winter CH4 and CO2 accumulation from a permafrost peatland pond is critical to spring thaw carbon emissions. *Wetlands*, *44*(7), 93. https://doi.org/10.1007/s13157-024-01852-1

Yvon-Durocher, G., Allen, A. P., Bastviken, D., Conrad, R., Gudasz, C., St-Pierre, A., et al. (2014). Methane fluxes show consistent temperature dependence across microbial to ecosystem scales. *Nature*, *507*(7493), 488–491. https://doi.org/10.1038/nature13164

Zhuang, Q., Guo, M., Melack, J. M., Lan, X., Tan, Z., Oh, Y., & Leung, L. R. (2023). Current and future global lake methane emissions: A process-based modeling analysis. *Journal of Geophysical Research: Biogeosciences*, *128*(3), e2022JG007137. https://doi.org/10.1029/2022JG007137

Zolkos, S., MacDonald, E., Hung, J. K. Y., Schade, J. D., Ludwig, S., Mann, P. J., et al. (2022). Physiographic controls and wildfire effects on aquatic biogeochemistry in tundra of the Yukon-Kuskokwim Delta, Alaska. *Journal of Geophysical Research: Biogeosciences*, *127*(8), e2022JG006891. https://doi.org/10.1029/2022JG006891